LETTER

doi:10.1038/nature23478

GLUTAMATE RECEPTOR–LIKE channels are essential for chemotaxis and reproduction in mosses

Carlos Ortiz-Ramírez[1]†, Erwan Michard[1,2], Alexander A. Simon[2], Daniel S. C. Damineli[2], Marcela Hernández-Coronado[1]†, Jörg D. Becker[1] & José A. Feijó[1,2]

Glutamate receptors are well characterized channels that mediate cell-to-cell communication during neurotransmission in animals, but their functional role in organisms without a nervous system remains unclear. In plants, genes of the GLUTAMATE RECEPTOR-LIKE (GLR) family have been implicated in defence against pathogens, reproduction, control of stomata aperture and light signal transduction[1–5]. However, the large number of GLR genes present in angiosperm genomes (20 to 70)[6] has prevented the observation of strong phenotypes in loss-of-function mutants. Here we show that in the basal land plant *Physcomitrella patens*, mutation of the GLR genes *GLR1* and *GLR2* causes failure of sperm cells to target the female reproductive organs. In addition, we show that GLR genes encode non-selective Ca^{2+}-permeable channels that can regulate cytoplasmic Ca^{2+} and are needed to induce the expression of a BELL1-like transcription factor essential for zygote development. Our work reveals functions for GLR channels in sperm chemotaxis and transcriptional regulation. Sperm chemotaxis is essential for fertilization in both animals and early land plants such as bryophytes and pteridophytes. Therefore, our results suggest that ionotropic glutamate receptors may have been conserved throughout plant evolution to mediate cell-to-cell communication during sexual reproduction.

Only two GLR genes have been identified in the moss *Physcomitrella*[7], and phylogenetic analyses showed that these genes are paralogues to *Arabidopsis* clade three[8]. As a first approach to determine the function of GLR genes in mosses, we complemented our previous transcriptomic analysis[9] to profile the expression of *P. patens GLR1* and *GLR2*. We purified mRNA from all tissues including archegonia, sperm cells and sporophytes isolated at three different developmental stages, and monitored *GLR1* and *GLR2* expression by quantitative reverse transcription PCR (qRT–PCR) (Fig. 1). *GLR1* transcript was detected in all tissues, with the highest expression in gametophores and young sporophytes. By contrast, *GLR2* has a very specific expression pattern that is limited to archegonia, sperm cells and mature sporophytes (Fig. 1a), suggestive of a role in sexual reproduction.

We then progressed to loss-of-function studies by generating single- and double-knockout mutants by homologous recombination (*glr1-19*, *glr2-11*; double mutant line referred as *glr1/2)*. Early developmental stages are characterized by the presence of haploid tip growing cells (caulonema and chloronema), and none of our mutant lines displayed any phenotypic defects in these cell types. Even when exposed to low Ca^{2+} conditions, growth was comparable between wild-type lines and *glr1/2* mutants (Extended Data Fig. 1a). This was unexpected since GLR mutations in *Arabidopsis* produced tip growth defects in pollen tubes[4]. Because caulonema filaments are the most active tip-growing cells in *Physcomitrella*, we preferentially induced their development to test whether tip growth was impaired in *glr1/2* mutants. However, caulonema cells grew normally (Extended Data Fig. 1b, c), suggesting that GLR function in apical growth is not conserved between angiosperms and bryophytes.

Importantly, in *Arabidopsis glr* mutants, pollen tube growth defects lead to male reproductive phenotypes[4]. Having this in mind and considering the transcriptomic profile of *P. patens GLR2*, we decided to investigate further whether *P. patens* GLR genes had a conserved role in reproduction. We induced the development of reproductive structures (gametangia) and quantified the production of sporophytes (the diploid zygotic structure) as a way to assess fertilization rates indirectly. Under our conditions, $56.3 \pm 11\%$ (mean $\pm$ s.d., unless otherwise specified) of wild-type gametophores develop mature sporophytes after 6 weeks of induction (Fig. 1c). Notably, all *P. patens glr* mutant lines produced far fewer sporophytes than wild-type lines (Fig. 1b). The percentage of gametophores with sporophytes in *glr1* decreased to $33 \pm 7\%$ and was even more severe in *glr2* and *glr1/2* double-knockout lines, with $17.9 \pm 3.9\%$ and $10.2 \pm 6.2\%$, respectively. Furthermore, the few sporophytes produced by the mutant lines showed delayed maturation (Fig. 1c), suggestive of a possible role in sporophyte developmental progression. These phenotypes cannot be attributed to defects in the formation of reproductive organs, because archegonia (organs that form the female gametes) and antheridia (the male counterpart) isolated from *glr1/2* mutants show the same morphology and developmental patterns as wild-type lines (Fig. 1b).

To determine the contribution of male and female gametes to the low sporophyte production rates observed in mutant lines, we carried out cross-fertilization experiments. We used transgenic lines expressing green and red fluorescent protein (GFP and RFP, respectively) as markers to discriminate between self-fertilized and hybrid sporophytes. First, we investigated whether sporophyte production rates could increase by crossing GFP-expressing wild-type plants with *glr1/2* mutants. Interestingly, $33.0 \pm 6.3\%$ of *glr1/2* gametophores produced sporophytes, almost all of them originating from outcrossing events (hybrid sporophytes) (Fig. 1d; Table 1). This observation supports the interpretation that wild-type sperm can fertilize mutant plants.

Notably, in this experimental setting, complementation depends solely on outcrossing efficiency. Therefore, as a reference we estimated natural outcrossing rates in wild-type plants and found that they were indeed similar to those reported in our first cross (Table 1). To show that *glr1/2* archegonia is capable of producing sporophytes at normal rates, we crossed this line with the more efficient *Physcomitrella* Villersexel outcrosser strain[10] expressing RFP (referred to as *Vsx* RFP). As a result, sporophyte production rates in *glr1/2* were even higher than wild-type lines ($72.0 \pm 18.9\%$), presenting a complete phenotypic rescue (Extended Data Fig. 1d, e).

We then performed the reverse crossing experiment to test whether *glr1/2* sperm were incapable of achieving fertilization. We found that outcrossing rates dropped markedly when the *glr1/2* mutant expressing

[1]Instituto Gulbenkian de Ciência, Oeiras, 2780-156, Portugal. [2]University of Maryland, Department of Cell Biology and Molecular Genetics, 0118 BioScience Research Building, College Park, Maryland 20742-5815, USA. †Present address: New York University, Department of Biology, Center for Genomics and Systems Biology, 12 Waverly Place, New York, New York 10003, USA.

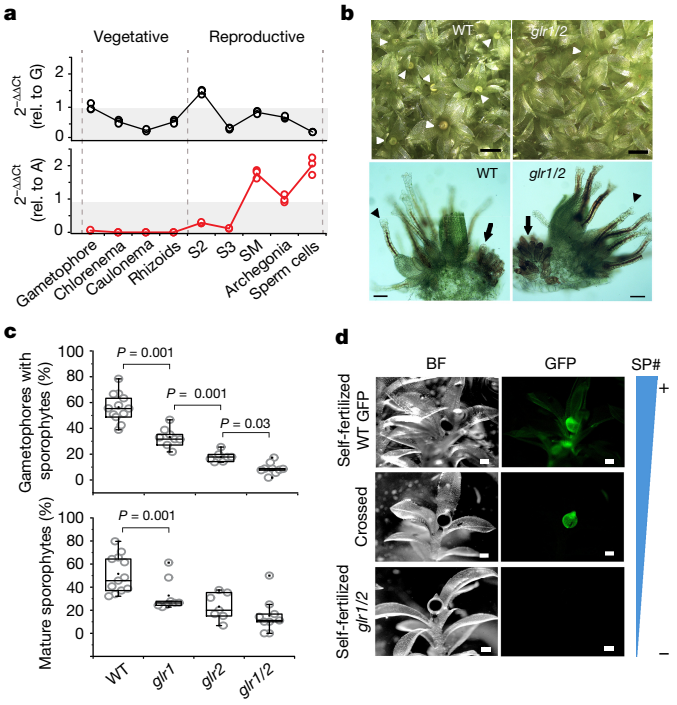

Figure 1 | *GLR* mutants have male reproductive phenotypes. **a**, Expression levels of *GLR1* (black line) and *GLR2* (red line) were determined by qRT–PCR analyses. Fold change expression values relative to gametophore (G) and archegonia (A) are shown. S2, 9-day-old sporophyte (d.o.s); S3, 18 d.o.s.; SM, 28 d.o.s. RNA from 3 biological replicates was used. Bold lines display the mean values from three technical replicates (open circles). **b**, Top, wild-type (WT) gametophores show more sporophytes (arrowheads) than *glr1/2* mutants. Bottom, images of archegonia (arrowheads) and antheridia (arrows) show that reproductive organs have normal development. Scale bars, 1 mm (top) and 50 μm (bottom). Images are representative of 3 images each. **c**, Quantification of sporophyte production in different genotypes. 100 gametophores were counted per sample. Data from several independent biological replicates. $n = 12$ (WT), $n = 8$ (*glr1*), $n = 7$ (*glr2*), $n = 8$ (*glr1/2*). *P* values obtained by unpaired two-tailed *t*-tests. Box plots range from 25th to 75th percentiles, black dots inside the box represent the mean, lines indicate outliers and black crosses represent the 1st and 99th percentiles. **d**, Self-fertilization events (top and bottom) and outcrossing events (middle) were identified in cross-fertilization experiments between wild-type GFP (paternal line) and *glr1/2* (maternal line). Sporophyte number (SP#) decreased markedly in self-fertilized *glr1/2*. BF, bright-field. Scale bars, 300 μm. Images are representative of 4 images.

GFP was crossed as the paternal line, with only $1.0 \pm 1.4\%$ of wild-type gametophores producing hybrid sporophytes (Table 1). These results unequivocally demonstrate that the phenotypic transmission of the GLR defect runs through the male by affecting sperm function in *glr1/2*.

We thus hypothesized that mutant sperm could be defective in their ability to navigate and perceive female cues. An *in vitro* sperm navigation assay was developed to test this possibility (see Methods and Extended Data Fig. 2a). We observed that wild-type sperm move with a helicoidal motion at an average speed of $16.7 \pm 3.4\,\mu m\ s^{-1}$ (Supplementary Video 1; Fig. 2f). Notably, a total of 2.6 ± 1.3 cells per released cluster (sperm cells are released in single clusters of approximately 150 cells) successfully contacted the archegonia opening, and 1.3 ± 1.1 cells managed to enter the archegonia channel (Supplementary Videos 3, 4 and Fig. 2a, b, d, e). By contrast, *glr1/2* sperm cells move faster than wild-type cells at an average speed of $23.2 \pm 10.8\,\mu m\ s^{-1}$ (Supplementary Video 2; Fig. 2f), and are far less efficient at targeting and entering the archegonia opening (0.63 ± 1.0 and 0.54 ± 0.9 sperm cells per cluster, respectively) (Supplementary Videos 5, 6 and Fig. 2a, c–e). The increased speed of mutant sperm cells might impinge in their inability to detect and/or respond to female cues. Such responses suggest changes in the trajectories of the cells that are expected to decrease their linear velocity. Given the random direction of sperm swimming, targeting archegonia is possible just by chance. Accordingly, none of the successful events from *glr1/2* cells showed sharp changes in direction in contrast to that observed for the wild-type cells. These results implicate *P. patens* GLRs in the control of sperm speed and turning motion in response to female cues, suggesting that even small modifications in one of these parameters is sufficient to reduce fertilization rates markedly.

Table 1 | Sporophyte production rates in cross-fertilization experiments

Crossed genotypes	Gametophores with sporophytes in female line (%)		
	From out-cross	From self-fertilization	Total
Wild-type GFP ♂ × wild-type ♀	28.1 ± 2.8	35.2 ± 11.6	63.3 ± 8.8
Wild-type GFP ♂ × *glr1/2* ♀	33 ± 6.3	0.9 ± 1.2	33.9 ± 7.6
glr1/2 GFP ♂ × wild-type ♀	1 ± 1.4	50.2 ± 6	51.3 ± 4.6

50 gametophores were analysed for each cross. Data are mean ± s.d. from two independent biological experiments. Male and female symbols are used to show how lines were crossed.

Because sperm motility and capacitation in animals is controlled in part by rises in free cytosolic Ca^{2+} concentration ($[Ca^{2+}]_{cyt}$)[11], we investigated whether *P. patens* GLRs could regulate $[Ca^{2+}]_{cyt}$ in moss sperm. We loaded wild-type and mutant sperm with the cytoplasmic Ca^{2+} indicator Fluo-4-AM and exposed the cells to medium containing numerous archegonia. Cytoplasmic $[Ca^{2+}]$ was lower in sperm cells lacking GLRs ($P < 0.001$, unequal variances *t*-test), indicating that these channels may affect sperm cell function through the regulation of Ca^{2+} concentration (Fig. 2g). To investigate this function further, we co-expressed *P. patens GLR1* (using the expression vector pCI-PpGLR1) with the Ca^{2+} genetic probe yellow CaMeleon 3.6 (YC3.6) in mammalian COS-7 cells. Cells transfected with pEF1-YC3.6 plus pCI-PpGLR1 had higher $[Ca^{2+}]_{cytoplasmic}$ than control cells transfected with pEF1-YC3.6 plus pCI empty vector (Fig. 2h, statistics in Extended Data Fig. 2b). Moreover, a clear increase in $[Ca^{2+}]_{cyt}$ was observed in GLR1-expressing cells when 14.5 mM Ca^{2+} was added to the bath solution (originally containing 1 mM EGTA) (Fig. 2h, i). These responses were recorded in the absence of any potential ligand in the bath solution, demonstrating a basal activity of GLR1. The addition of the cation channel blocker gadolinium (Gd^{3+}) at 1 mM abolished the response to external Ca^{2+} (Fig. 2h, i). Note that Gd^{3+} did not decrease basal $[Ca^{2+}]_{cytoplasmic}$, which remained higher than in control cells (Fig. 2h, i), suggesting that the kinetics of cytosolic Ca^{2+} extrusion and basal $[Ca^{2+}]_{cyt}$ adjustment in COS-7 cells is considerably slower than our 7-minute-long experiment.

While the previous results are sufficient to explain the reduced rates of fertilization observed in *glr1/2* mutants, defects in sporophyte maturation remained unaccounted for. As part of their normal maturation process, sporophytes undergo meiosis to produce large numbers of spores. To determine whether spore production was affected in the loss-of-function mutant, we isolated them and analysed their size, morphology and numbers. The *glr1/2* sporophytes produced smaller spores and in fewer numbers (Fig. 3a–c), indicating a role in sporophyte development. Notably, there is evidence that some ion channels regulating Ca^{2+} signalling events can affect development by inducing the expression of transcription factors[12,13]. With this in mind, we used microarrays to analyse the transcriptome of wild-type and *glr1/2* mutant reproductive organs isolated 16 days after gametangia induction. At this time, early embryos are expected to develop[9]. Microarray analysis revealed that several transcripts were significantly up and downregulated in *glr1/2*, implicating GLR activity in the modulation of gene expression. Although it was not possible to distinguish in which reproductive structure the transcripts were produced, we found the sporophyte-associated BELL1 transcription factor homologue among the most significantly down-

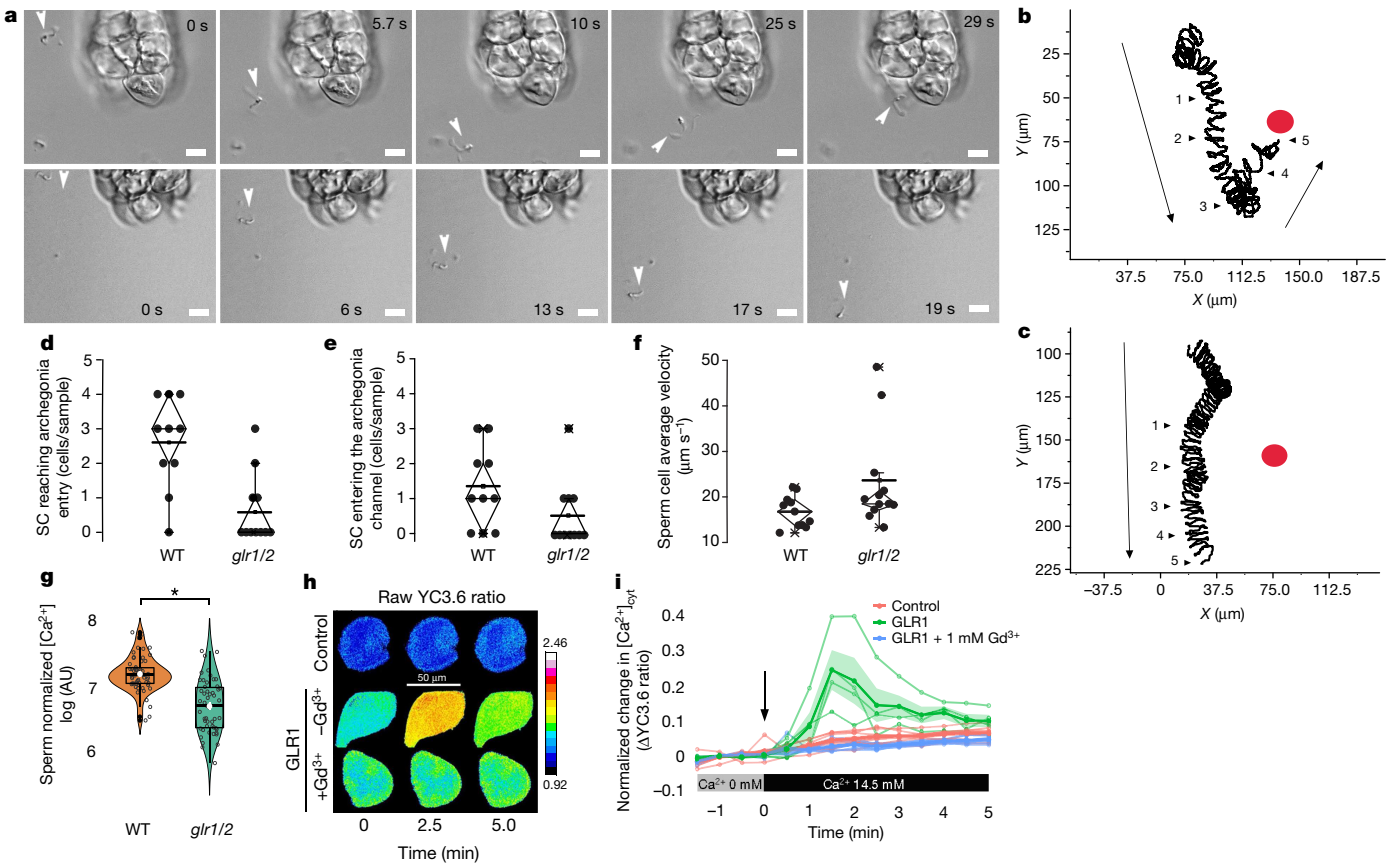

Figure 2 | Sperm cells from *glr1/2* fail to reach the archegonia entrance. **a**, Swimming behaviour in wild-type (top) and *glr1/2* mutant (bottom) sperm cells. Arrowheads indicate sperm position and direction. Scale bars, 10 µm. Frames are representative of 5 similar videos. **b**, **c**, Comparison between wild-type (**b**) and *glr1/2* (**c**) sperm-cell trajectories. Data are representative of 10 independent biological replicates. Numbers indicate the sperm-cell position when the frames presented in **a** were recorded, corresponding to frames 1 to 5 from left to right. Red circles represent archegonia entrance, and arrows indicate sperm forward movement direction. **d**, Number of sperm cells (SC) reaching the archegonia entrance. Wild-type sperm was more efficient at reaching archegonia. $P = 0.001$, two-tailed unpaired *t*-test. $n = 10$ (WT), $n = 11$ (*glr1/2*). **e**, Wild-type sperm cells are also more successful than *glr1/2* mutant cells at entering into the archegonia opening. $P = 0.05$, Mann–Whitney rank sum test. $n = 10$ (WT), $n = 11$ (*glr1/2*). **f**, Mutant sperm cells move faster than wild-type sperm. $P = 0.037$, one-tailed unpaired *t*-test. $n = 11$ (WT), $n = 12$ (*glr1/2*); biological replicates. Bold lines in **d**–**f** represent mean values. **g**, The cytoplasmic Ca^{2+} concentration is higher in wild-type sperm than in mutant sperm. $P = 6 \times 10^{-11}$, unequal variances *t*-test. The peak of the signal for each cell is shown in grey circles for wild-type sperm. $n = 59$ (WT), $n = 61$ (*glr1/2*), technical replicates. Violin plots show curves of density estimates, and boxplot range represents the s.e.m. White points represent the mean and lines indicate outliers. **h**, Cytosolic Ca^{2+} concentration monitored with yellow CaMeleon 3.6. Typical YC3.6 ratio for control cells (pCI empty vector + pEF1-YC3.6) (top, representative of 7 images), and cells expressing *GLR1* (pCI-PpGLR1 + pEF1-YC3.6) without Gd^{3+} (middle, representative of 4 images) or with Gd^{3+} (1 mM; bottom, representative of 7 images) at time 0, 2.5 and 5.0 min after the addition of Ca^{2+} (14.5 mM) (colour wedge depicts raw YC3.6 ratio). **i**, Time course of the change in cytosolic Ca^{2+} concentration before and after the addition of Ca^{2+} in the bath (indicated by the arrow). The *y* axis shows values of YC3.6 ratio (cpVenus/CFP ratio) minus the average ratio before the Ca^{2+} increase. Cells expressing GLR1 (green line, $n = 4$), control cells (red line, $n = 7$), and cells expressing GLR1 exposed to Gd^{3+} (1 mM; blue line, $n = 7$) are shown. The bold lines display the mean response for each treatment, the shaded area denotes the s.e.m., and thin lines denote individual replicates. EGTA (1 mM) was added to the medium without Ca^{2+}.

regulated genes (Extended Data Table 1 and Supplementary Table 2). Members of the BELL1 family are known to control egg cell and sporophyte development in *Arabidopsis*[14–17], as well as the regulation of the diploid genetic program in *Chlamydomonas* and *Physcomitrella*[18,19]. In light of these results, we hypothesized that the low levels of *P. patens* BELL1 detected in the mutant were responsible for the sporophyte developmental defects. To test this hypothesis, we attempted to rescue *glr1/2* by driving the expression of *BELL1* with the promoter of *GLR2*. This promoter is specifically expressed in reproductive organs and sporophytes, preventing possible artefacts of overexpression at other developmental stages. Using homologous recombination, the *BELL1* coding sequence was inserted *in situ* immediately downstream of the *GLR2* promoter. This line is referred to as *GLR2::BELL1*. In accordance with our hypothesis, sporophyte analyses of *GLR2::BELL1* showed a significant increase in the number of spores per sporophyte as well as in spore area, which increased from 4,161.1 ± 1,024 in *glr1/2* to 6,302 ± 1,636 in *GLR2::BELL1* and from 200.9 ± 66 µm^2 to 428.1 ± 185 µm^2, respectively (Fig. 3b, c). This rescue indicates not only that the *BELL1* gene has an important role in sporophyte development, but also that *GLR2* may act upstream of a signalling pathway that regulates the expression of this transcription factor. In line with this, gene network analysis performed using the PlaNET tool[20] showed that many transcription factor genes are associated with *GLR2*, but not with *GLR1* (Extended Data Fig. 3). Most of them have homologues known to control sporophyte development in angiosperms. Gene Ontology analysis confirmed that the *GLR2* gene network is mainly associated with transcriptional regulation and protein kinase activity (Extended Data Fig. 3 and Supplementary Table 3). Importantly, sporophyte production rates did not increase in the *GLR2::BELL1* complementation line (Extended Data Fig. 2c) showing that GLR activity affects fertilization and sporophyte development through independent mechanisms.

Finally, given their conspicuous phenotypic effects in reproduction, we further aimed at establishing the function of *Physcomitrella* GLRs as

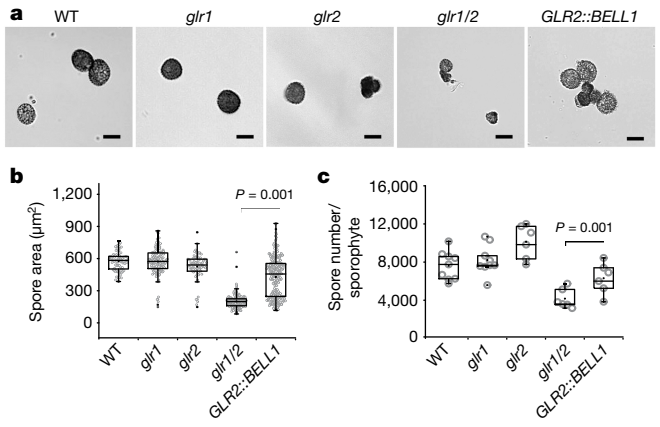

Figure 3 | *BELL1* influence sporophyte spore production and size. **a**, Pictures of isolated spores showing that *glr1/2* produced smaller spores than wild type. *glr1/2* spores also presented irregular shape and tend to stick together. Images are representative of at least 20 images. **b**, Measurements of spore area. Spores from 3 biological replicates were pooled and individual spores were measured. $n = 82$ (WT), $n = 62$ (*glr1*), $n = 75$ (*glr2*), $n = 173$ (*glr1/2*), and $n = 284$ (*GLR2::BELL1*). **c**, Quantification of the number of spores per sporophyte shows that *glr1/2* produced less spores than wild type and single mutants. Several sporophytes produced by independent inductions (biological replicates) were used for quantification. $n = 9$ (wild type), $n = 6$ (*glr1*, *glr2*, *glr1/2* and *GLR2::BELL1*). In **b** and **c**, box plots range from 25th to 75th percentiles, black dots inside the box represent the mean, and lines indicate outliers. Complementation of *glr1/2* (last bar in **b** and **c**) caused a significant increase in spore size and numbers. *P* values obtained by Mann–Whitney *U* test (**b**) and *t*-test (**c**). Scale bars, 25 µm.

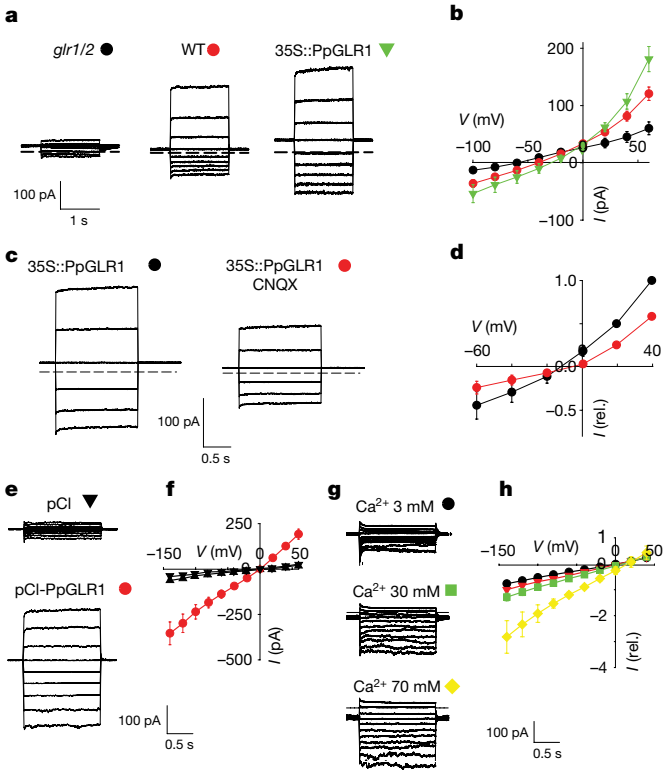

Figure 4 | GLRs are Ca^{2+}-permeable channels in the plasma membrane. **a**, Typical currents recorded by patch-clamp (whole-cell configuration) in protoplasts from protonema of *glr1/2*, wild-type and the 35S::PpGLR1 overexpressor (see Methods). **b**, Current–voltage curves of stationary currents recorded in experiments shown in **a**. $n = 19$ (*glr1/2*); $n = 40$ (WT); $n = 20$ (35S::PpGLR1). **c**, Effect of 50 µM CNQX on typical currents recorded in protoplasts from 35S::PpGLR1 ($n = 5$). **d**, Respective standardized current–voltage before (black circles) and after (red circles) application of CNQX ($n = 5$). **e**, Typical currents recorded in COS-7 cells transfected with the pCI empty vector (top) and pCI-PpGLR1 vector (bottom) recorded in standard COS-7 cell solutions (see Methods). **f**, Current–voltage curves of control COS-7 cells transfected with the screening pIRES-CD8 vector (black upwards triangle, $n = 5$) or with pIRES-CD8 plus pCI empty vector (black downwards triangle, $n = 7$), and cells transfected with pIRES-CD8 plus pCI-PpGLR1 (red circles, $n = 13$). **g**, Typical currents recorded from COS-7 cells transfected with pCI-PpGLR1 under successive perfusion of external solutions with increasing Ca^{2+} concentrations (3, 10, 30 and 70 mM) while maintaining constant Cl^-. **h**, Standardized current–voltage curves of experiments presented in **g**. Ca^{2+} 3 mM (black circles, $n = 5$), Ca^{2+} 10 mM (red triangle, $n = 5$), Ca^{2+} 30 mM (green square, $n = 5$), Ca^{2+} 70 mM (yellow diamond, $n = 3$). Error bars denote s.e.m. In all cases, *n* represents biological replicates.

ionotropic channels using the patch-clamp technique. We first investigated whether *GLR1* was present on the plasma membrane of moss cells by measuring whole-cell ion currents in protonema isolated protoplasts (Fig. 4). Under our conditions (see Methods), instantaneous currents were significantly higher in wild-type protoplasts than in *glr1/2* mutants from −100 to +60 mV (Fig. 4a, b). Moreover, protoplasts stably overexpressing *GLR1* cDNA under the control of the 35S promoter exhibited significantly stronger currents than wild-type protoplasts (Fig. 4a, b). These currents were inhibited by Gd^{3+} (0.5–1.0 mM; Extended Data Fig. 4a, b) and by the ionotropic glutamate receptor (iGluR) antagonists 6-cyano-7-nitroquinoxaline-2,3-dione (CNQX) (50 µM; Fig. 4c, d) and 2-amino-5-phosphonovalerate (AP_5) (200 µM; Extended Data Fig. 4c, d).

We further characterized GLR1 conductivity in mammalian COS-7 cells. Cells expressing *P. patens GLR1* had higher currents than control cells (approximately 300 pA at −100 mV) (Fig. 4e, f) and they were inhibited by the same iGluR antagonists used in protoplasts (Extended Data Fig. 5). Cationic conductance increased in both COS-7 cells and protoplasts after extracellular increases in Na^+ concentration (10–110 mM in protoplasts, 0–130 mM in COS-7 cells), suggesting cationic permeability (Extended Data Fig. 6). When Ca^{2+} and Cl^- were used as the only charge carriers in the solution, a clear current increase was observed with perfusion of increasing Ca^{2+} concentrations (3, 10, 30, 70 mM), while maintaining Cl^- constant, demonstrating Ca^{2+} permeability of GLR1 (Fig. 4g, h).

We thus propose that both sperm chemotaxis and transcriptional modulation of BELL1 are dependent on GLR-mediated regulation of $[Ca^{2+}]_{cyt}$. Because the expression of several ionotropic GLRs has been detected in sperm cells of plants belonging to different phylogenetic groups[21], as well as in mammalian sperm[22], ionotropic glutamate receptors may have a conserved role in male gamete signal perception/steering common to bryophytes, vascular plants and animals[4].

Online Content Methods, along with any additional Extended Data display items and Source Data, are available in the online version of the paper; references unique to these sections appear only in the online paper.

Received 28 December 2016; accepted 14 July 2017.
Published online 24 July 2017.

1. Forde, B. G. & Roberts, M. R. Glutamate receptor-like channels in plants: a role as amino acid sensors in plant defence? *F1000Prime Rep.* **6,** 37 (2014).
2. Cho, D. *et al.* De-regulated expression of the plant glutamate receptor homolog AtGLR3.1 impairs long-term Ca^{2+}-programmed stomatal closure. *Plant J.* **58,** 437–449 (2009).
3. Lam, H. M. *et al.* Glutamate-receptor genes in plants. *Nature* **396,** 125–126 (1998).
4. Michard, E. *et al.* Glutamate receptor-like genes form Ca^{2+} channels in pollen tubes and are regulated by pistil D-serine. *Science* **332,** 434–437 (2011).
5. Mousavi, S. A., Chauvin, A., Pascaud, F., Kellenberger, S. & Farmer, E. E. GLUTAMATE RECEPTOR-LIKE genes mediate leaf-to-leaf wound signalling. *Nature* **500,** 422–426 (2013).
6. Chiu, J. C. *et al.* Phylogenetic and expression analysis of the glutamate-receptor-like gene family in *Arabidopsis thaliana*. *Mol. Biol. Evol.* **19,** 1066–1082 (2002).
7. Verret, F., Wheeler, G., Taylor, A. R., Farnham, G. & Brownlee, C. Calcium channels in photosynthetic eukaryotes: implications for evolution of calcium-based signalling. *New Phytol.* **187,** 23–43 (2010).

8. De Bortoli, S., Teardo, E., Szabò, I., Morosinotto, T. & Alboresi, A. Evolutionary insight into the ionotropic glutamate receptor superfamily of photosynthetic organisms. *Biophys. Chem.* **218,** 14–26 (2016).
9. Ortiz-Ramírez, C. *et al.* A transcriptome atlas of *Physcomitrella patens* provides insights into the evolution and development of land plants. *Mol. Plant* **9,** 205–220 (2016).
10. Perroud, P. F., Cove, D. J., Quatrano, R. S. & McDaniel, S. F. An experimental method to facilitate the identification of hybrid sporophytes in the moss *Physcomitrella patens* using fluorescent tagged lines. *New Phytol*. **191,** 301–306 (2011).
11. Ren, D. *et al.* A sperm ion channel required for sperm motility and male fertility. *Nature* **413,** 603–609 (2001).
12. Lilienbaum, A. & Israël, A. From calcium to NF-κB signaling pathways in neurons. *Mol. Cell. Biol.* **23,** 2680–2698 (2003).
13. Hogan, P. G., Chen, L., Nardone, J. & Rao, A. Transcriptional regulation by calcium, calcineurin, and NFAT. *Genes Dev.* **17,** 2205–2232 (2003).
14. Rutjens, B. *et al.* Shoot apical meristem function in *Arabidopsis* requires the combined activities of three BEL1-like homeodomain proteins. *Plant J*. **58,** 641–654 (2009).
15. Reiser, L. *et al.* The *BELL1* gene encodes a homeodomain protein involved in pattern formation in the *Arabidopsis* ovule primordium. *Cell* **83,** 735–742 (1995).
16. Brambilla, V. *et al.* Genetic and molecular interactions between BELL1 and MADS box factors support ovule development in *Arabidopsis*. *Plant Cell* **19,** 2544–2556 (2007).
17. Bowman, J. L., Sakakibara, K., Furumizu, C. & Dierschke, T. Evolution in the cycles of life. *Annu. Rev. Genet.* **50,** 133–154 (2016).
18. Horst, N. A. *et al.* A single homeobox gene triggers phase transition, embryogenesis and asexual reproduction. *Nat. Plants* **2,** 15209 (2016).
19. Lee, J. H., Lin, H., Joo, S. & Goodenough, U. Early sexual origins of homeoprotein heterodimerization and evolution of the plant KNOX/BELL family. *Cell* **133,** 829–840 (2008).
20. Mutwil, M. *et al.* PlaNet: combined sequence and expression comparisons across plant networks derived from seven species. *Plant Cell* **23,** 895–910 (2011).
21. Borges, F. *et al.* Comparative transcriptomics of *Arabidopsis* sperm cells. *Plant Physiol.* **148,** 1168–1181 (2008).
22. Hu, J. H. *et al.* Identification of glutamate receptors and transporters in mouse and human sperm. *J. Androl*. **25,** 140–146 (2004).

Supplementary Information is available in the online version of the paper.

Acknowledgements We thank P. F. Perroud for the Gransden GFP and Villersexel RFP lines; L. Dolan and T. Tan for the pBNRF, pBHrev and p108GW35S vectors; M. Hasebe for the pTN83 construct; S. Rensing for providing us access to the Nimblegen_Ppat_SR_-exp_HX12 array and the Institute for Research in Biomedicine (IRB)/Functional Genomics Core (FGC) (Barcelona) for microarray processing; J. Kudla for the pEF1-YC3.6 vector. C.O.R. and M.H.C. acknowledge fellowships from MarieCurie ITN-Plant Origins (FP7-PEOPLE-ITN-2008). J.A.F. acknowledges grants from the Fundação para a Ciêncua e Tecnologia (FCT)-Portugal (BEX-BCM/0376/2012; PTDC/BIA-PLA/4018/2012) and the National Science Foundation (NSF)-US (MCB 1616437/2016).

Author Contributions C.O.R. was involved in generating all experimental data except electrophysiology. E.M. and A.A.S. performed the electrophysiology. D.S.C.D. performed image and data analysis. M.H.C. and J.D.B. isolated sperm cells, purified RNA and analysed transcriptomic data. J.A.F. conceived the project. J.A.F. and C.O.R. wrote the manuscript and conceived all experiments. All authors discussed and improved the manuscript.

Author Information Reprints and permissions information is available at www.nature.com/reprints. The authors declare no competing financial interests. Readers are welcome to comment on the online version of the paper. Publisher's note: Springer Nature remains neutral with regard to jurisdictional claims in published maps and institutional affiliations. Correspondence and requests for materials should be addressed to J.A.F. (jfeijo@umd.edu).

Reviewer Information *Nature* thanks J. Kudla and the other anonymous reviewer(s) for their contribution to the peer review of this work.

METHODS

Data reporting. The experiments were not randomized, and investigators were not blinded to allocation during experiments and outcome assessment.

Plant material and growth conditions. The Gransden wild-type strain from *Physcomitrella patens* (Bruch and Schimp)[23] was used for this study. Plant material was routinely grown on Petri dishes containing KNOPS media[24] supplemented with 0.5 g l^{-1} ammonium tartrate dibasic and 5 g l^{-1} glucose (Sigma-Aldrich) at 25 °C, 50% humidity and 16 h light (light intensity 90–100 μmol m^{-2} s^{-1}). Vegetative propagation was maintained by subculture every 6–7 days by mechanical disruption of plant tissue using a tissue disruptor (TissueRuptor; Quiagen) leading to predominant growth of chloronema. For gametangia and sporophyte development, protonema was cultured on sterile peat pellets (Jiffy-7; Jiffy Products) in plant culture boxes for 28 days, until gametophores were fully mature. Water was supplied to the bottom of each box containing four pellets and samples were transferred to 17 °C, 8 h light and 50% humidity (light intensity 80–85 μmol m^{-2} s^{-1}) to induce the development of reproductive structures[25]. Further development of the sporophyte was conducted under these conditions.

Protoplast preparation. Protoplasts were prepared from protonema grown over 4 days in solid KNOPS media. Approximately 200 μl of fresh protonema was harvested and incubated for 30 min at 20 °C in a solution of 500 mM D-mannitol plus 1% driselase (Sigma-Aldrich) that was centrifuged for 5 min (10,000 g). Protoplasts were filtered (50 μm mesh), pelleted (5 min centrifugation at 250*g*) and washed twice in 500 mM D-mannitol. They were finally transferred to the bath solution for patch-clamp (see below), stored in the dark at 4 °C and studied by the patch-clamp technique within the next 3 h. Protoplasts were selected under the microscope (20× magnification).

COS-7 cell transfection. COS-7 cells (provided by ATCC) were used in low passage numbers (less than 10). The *GLR1* coding sequence was introduced into the pCI vector (Promega). COS-7 cells were plated at a density of 50% confluence in 35-mm-diameter dishes and immediately transfected using FugeneHD (Promega) as specified by the supplier. pIRES-CD8 was co-transfected with pCI-PpGLR1 to select transfected cells[26]. pIRES-CD8 is a pCI-derived vector used here for the expression of the CD8 protein as a marker. For the transfection mix, we used 7 μl of FugeneHD, 1.5 μg of pCI-PpGLR1 and 0.2 μg of pIRES-CD8 in 150 μl water. Cells were transferred to new Petri dishes 24 h after transfection (by trypsin treatment), at low density for patch-clamp study. Cells were analysed 36–48 h after transfection. Transfected cells were detected with the anti-CD8 antibody-coated bead method (Dynabeads CD8, Thermofisher)[27]. Authenticated COS-7 cell lines used in all experiments were purchased from ATCC (https://www.atcc.org). No further testing for mycoplasma was done in our laboratory after purchase.

Patch-clamp experiments. Pipettes were pulled with a P97 puller (Sutter Instrument) to a resistance of: 3–5 MΩ for COS-7 cells, and 15 MΩ for protoplasts in the respective bath solutions. Currents were recorded after establishing the whole-cell configuration and filtered at 1–2 kHz with a sampling frequency of 2–4 kHz using an Axopatch 200A amplifier, a DigiData 1322A AD-converter (Molecular Devices) and WinWCP software (http://spider.science.strath.ac.uk/sipbs/software_ses.htm). 6-cyano-7-nitroquinoxaline-2,3-dione disodium salt hydrate (CNQX, Santa Cruz Biotech) (100 μM) was eventually added to the bath solution. For whole-cell recordings, the pipette solution contained 140 mM NaCl, 3 mM $MgCl_2$, 5 mM EGTA, and 10 mM Bis-Tris propane, pH 7.2 (HEPES). For COS-7 cells, the bath solution contained 10 mM NaCl, 130 mM *N*-methyl-D-glucamine-Cl, 5 mM $CaCl_2$, and 10 mM Bis-Tris propane, pH 6.0 (MES). For protoplasts: 10 mM NaCl, 100 mM *N*-methyl-D-glucamine-Cl, 20 mM $CaCl_2$, and 10 mM Bis-Tris propane, pH 6.0 (MES). For protoplasts recordings, bath and pipette solutions were adjusted to 500 mOsmol kg^{-1} with D-mannitol. Voltage protocol: 1.5 s pulses from −100 or −140 mV to +40 or +60 mV (20 mV steps), holding potential 0 mV. The alternative internal solution for COS-7 cells (Fig. 4g, h) consisted of 10 mM HEPES, 3 mM $MgCl_2$, 5 mM EGTA and 1 mM $CaCl_2$ for a final free Ca^{2+} concentration of less than 100 nM (http://web.stanford.edu/~cpatton/webmaxcS). Pipette solutions were adjusted to pH 7.3 with Bis-Tris propane and to 350 mOsmol kg^{-1} with D-mannitol. Alternative external solutions for COS cell experiments were (1) 3 mM $CaCl_2$; or (2) 7 mM, 27 mM or 67 mM calcium D-gluconate with 3 mM $CaCl_2$. External solutions also contained 10 mM Bis-Tris propane and adjusted to pH 7.3 with HEPES and 350 mOsmol kg^{-1} with D-mannitol. Liquid junction potentials were corrected offline with Clampex 10.0.

Ca^{2+} imaging in COS-7 cells. COS-7 cells were co-transfected with 0.5 μg pEF1-YC3.6 plus 1 μg pCI-PpGLR1 as described above. Cells were detached by trypsin and transferred the day before imaging to 35 mm Petri dishes with 14 mm glass coverslip (MatTek). Cells were washed three times with the following bath solution: EGTA (1 mM), BTP (10 mM) pH 7.3 (HEPES), with or without $GdCl_3$ (1 mM) adjusted to 350 mOsmol with D-mannitol. In a first step, images were acquired with 500 μl bath solution. After 2.5 min, 500 μl of a solution containing $CaCl_2$ (30 mM) and BTP (10 mM) at pH 7.3 (HEPES), with or without $GdCl_3$ (1 mM) adjusted to 350 mOsmol with D-mannitol was added to the dish. Cells expressing YC3.6 were imaged at room temperature using a DeltaVision Elite Deconvolution/TIRF microscope system (Olympus inverted IX-71) under a 60× lens (1.2NA UPLSAPO water lens/WD 0.28 mm). Xenon lamp from the DeltaVision system was used with CFP excitation filter (415–445 nm). Two simultaneous emission records were captured, for CFP emission (455–485 nm) and for cpVenus emission (520–550 nm). To minimize bleaching, the laser was set to 2%, and cpVenus and CFP imaging were recorded with 0.3 and 0.2 s exposure times, respectively. A time-lapse acquisition was performed with a sampling interval of 30 s. Images were processed using ImageJ (http://imagej.net/Welcome). Ratios were obtained after background subtraction and signal clipping using the 'ratio-plus' plug-in for ImageJ. Signals for each channel were averaged from a circle in the middle of the cell (approximately 100–200 pixels in diameter depending on the size of the cell). The cpVenus/CFP ratio was obtained by dividing the emission recorded for cpVenus (520–550 nm) by the one recorded for CFP (455–485 nm). No significant bleaching or drift or the ratio was observed our experimental conditions. For qualitative analysis, images were processed in ImageJ with the Gaussian blur filter set to a radius of 0.75 pixels. Authenticated COS-7 cell lines used in all experiments were purchased from ATCC (https://www.atcc.org). No further testing for mycoplasma was done in our laboratory after purchase.

Tissue Isolation for RNA extraction. Triplicates for the different tissue samples were isolated from wild-type Gransden strain according to the particularities of each tissue. Archegonia were isolated from gametophores exposed to short day conditions for 15 days. Dissection was done manually under the stereoscope (SMZ800; Nikon) and placed into Trizol. At this point maturity was ensured and only closed organs were selected. A total of 300 archegonia were used per replicate to isolate RNA. Sporophytes from different developmental stages were manually collected. Included stages were designated 'S2', 'S3' and 'SM', as defined previously[9]. Gametophores at the specific time points described above were dissected under the stereoscope and only the sporophytes fitting the desired morphological stage were isolated. At stage S2, the separation from archegonia tissue is not possible with our isolation methods and in order to maintain the comparative capabilities of our set, the residual archegonium was attached to all sporophytes collected. Samples were stored directly in Trizol. Approximately 25 sporophytes from each developmental stage were used for RNA extraction.

Caulonema development was induced by growing protonema under dark conditions in vertical KNOPS plates for 5 days, while chloronema was produced under normal conditions (16 h light/8 h dark). Both filaments were cut manually under a stereoscope (SMZ800; Nikon) and identity was confirmed by looking at the cell division plates. Tissue was directly placed in Trizol until RNA extraction. Rhizoids were harvested from gametophores grown in Magenta boxes (Sigma-Aldrich) containing KNOPS minimal medium[24] under normal conditions (16 h light/8 h dark). Around 100 gametophores per replicate were isolated, and the entire rhizoids were manually dissected with a razor blade under a stereomicroscope (SMZ800; Nikon). Isolated rhizoids were frozen in liquid nitrogen right after dissection.

Gametophores grown on sterile peat pellets (Jiffy-7; Jiffy Products) for 3 weeks were isolated manually and placed on Trizol for subsequent RNA extraction.

For sperm cell isolation, mature antheridia were manually dissected from gametophores at day 15 after induction. More than 50 antheridia per preparation were placed on a coverslip with 50 μl of sterile MilliQ water, where sperm release occurred naturally after few minutes. Using micromanipulators (CellTram; Eppendrof) attached to an inverted microscope (DMIRE2; Leica Microsystems), the clusters of cells were collected with microcapillaries. The collected sperm was placed directly into Trizol, frozen in liquid nitrogen and stored at −80 °C until use. For RNA extraction, 200–400 clusters were used per replicate and four replicates were generated.

RNA purification and cDNA synthesis. RNA from all samples was isolated and purified using columns (Direct-Zol; Zymo Research) following manufacturer's instructions. Samples were treated with TURBO DNase (Ambion, Life Technologies) at 37 °C for 30 min. RNA integrity and quantity were assessed on a Bioanalyzer using a 6000 Pico Assay (Agilent 2100; Agilent Technologies). On average, 7.5 ng of RNA was used to synthetize cDNA using an amplification kit (Ovation Pico WTA System V2; NuGen Technologies). The cDNA concentration obtained from all samples was roughly in the same range (180–260 ng μl^{-1}) and further quality controls were performed using a Bioanalyzer.

Determination of GLRs expression levels by qRT–PCR. cDNA was synthetized using RNA isolated from individual *Physcomitrella* tissues as described before. 1 ng of cDNA was used per reaction, 10 μl of enzyme mix (SYBR Green supermix; Bio Rad), 5 μl of each primer solution at 0.3 μM and 5 μl of diluted DNA. Each plate contained three technical replicates of every sample for each set of primers. We used the following primers for amplification qCR001/qCR002 for *GLR1*; qCR003/qCR004 for *GLR2* and qCR005/qCR006 for α-tubulin (*TUB*) (Supplementary Table 1). The thermal cycling protocol was as follows: initial 50 °C for 2 min, denaturation

for 10 min at 95 °C followed by 40 cycles of 30 s at 95 °C, 1 min at 59 °C and 30 s s at 72 °C. We obtained C_t values using the program SDS 2.4 or with Bio-Rad CFX Manager with default threshold settings. Experiments were carried out in an ABI7900HT system (Applied Biosystems).

Constructs and *P. patens* transformation. *GLR* knockout mutants were generated by homologous recombination using the G418 and hygromycin-resistance cassettes to replace the gene of interest. Genomic sequences of approximately 600 bp upstream and downstream of *GLR1* (Pp1s56_31V6) and *GLR2* (Pp1s253_26 V6) coding regions were amplified by PCR. To generate the plasmid used to replace *GLR1* genomic coding sequence, we amplified the flanking regions of the gene with the primers oCR003/oCR004 (upstream region), and oCR005/oCR06 (downstream region). Amplified flanking fragments were cloned into pBNRF vector flanking the G418 cassette using SalI and BamHI, and SpeI and AscI for upstream and downstream regions respectively. Plasmid was linearized to transform *Physcomitrella* protoplasts. Two rounds of antibiotic selection were done: during the first round, regenerated protoplasts were transferred to KNOPS medium with geneticin (G418), resistant colonies were transferred back to medium without antibiotics and grown for further 10 days before going to the second 10 day antibiotic selection. After final selection, DNA was extracted from stable resistant colonies and used for PCR amplification reactions of the *GLR1* gene. Colonies in which the presence of the genes could not be detected were selected as being putative knockouts and confirmed for the correct insertion of the resistance cassette by further PCR experiments (Extended Data Fig. 7a, c). Three independent knockout colonies were generated for *glr1* (*glr1-19*, *glr1-8* and *gl1-14*).

To generate *glr1/2* double knockout, we amplified the flanking regions of *GLR2* using the primers oCR015/oCR016 and oCR017/oCR018 for upstream and downstream regions, respectively, and cloned them into the pBHrev plasmid flanking the hygromicin-resistance cassette. Cloning was done using AscI and SpeI (upstream fragment), and SmaI and XbaI (downstream fragment) restriction enzymes. The plasmid was linearized and used to transform protoplasts obtained from the *glr1-19* mutant line. Selection and genotyping of stable mutants was done as before (Extended Data Fig. 7b, d). For detection of the *GLR1* gene we used the oCR001/oCR002 primer pair, and for the *GLR2* gene we used the oCR013/oCR014 primer pair. Three independent double-knockout colonies were generated (*glr1/2-63*, *glr1/2-11* and *glr1/2-16*) (Extended Data Fig. 7b, d). Confirmed independent mutant lines for single and double knockout mutants were phenotyped (quantification of sporophyte production), confirming that deletion of GLR genes had a similar effect in all lines with the same mutant background (Extended Data Fig. 8a, b). The phenotypes presented in the results section correspond to the *glr1-19* single-knockout and *glr1/2-11* double-knockout lines, except for microarray experiments in which *glr1/2-63* was used.

Constitutively overexpressing the *GLR1* line (35S::PpGLR1) was generated by amplifying the *GLR1* coding region from protonema cDNA with the primer pair oCR023/oCR024 and cloning this region into the Gateway pDONR 221 vector (Invitrogen). The *GLR1* coding region was then subcloned into the p108GW35S plasmid, which carries the 108 locus of *Physcomitrella*, by LR reaction using an enzyme mix (Gateway LR Clonase II enzyme mix; Invitrogen). The resulting vector was used for protoplast transformation and geneticin-resistant colonies were selected as before. Overexpression of *GLR1* in stable colonies was confirmed by RT–PCR using the primers oCR001/oCR002 and oCR044/oCR045 for *GLR1* and *TUB* amplification, respectively (Extended Data Fig. 9e). The 35S::PpGLR1-2 line was used for subsequent experiments.

Generation of the *glr1/2* line constitutively expressing GFP (*glr1/2* GFP) was done by crossing the double-knockout line with a transgenic line overexpressing GFP under the 2×35S promoter (gift from P. Perroud). After crossing these lines, hybrid sporophytes produced by *glr1/2* were identified under a fluorescent stereo microscope (Zeiss Stero Lumar) and collected. Spores obtained from hybrid sporophytes were germinated resulting in protonemal colonies. Those colonies positive for GFP fluorescence were selected and genotyped. We used primer pairs oCR001/oCR002 and oCR013/oCR014 for amplifying *GLR1* and *GLR2* genes, respectively, and further selected the colonies lacking both genes. We obtained four *glr1/2* GFP-independent lines, and only used the colony with the highest fluorescence intensity for performing experiments.

A *glr2* single-knockout line in which the *GLR2* coding sequence was replaced by the beta-glucuronidase reporter gene (*GUS*) was generated by homologous recombination. The flanking regions (approximately 700 bp) of *GLR2* were amplified with primers oCR034/oCR035 and oCR036/oCR037 for upstream and downstream regions, respectively. Both fragments were cloned into the pTN83 plasmid flanking the *GUS* gene, the nopaline synthase polyadenylation signal (Tnos) and the geneticin-resistant cassette using NotI and BamHI restriction enzymes (upstream flanking fragment) and EcoRI and SalI (downstream fragment). Plasmids were linearized and protoplast transformation, selection and genotyping were done as before (Extended Data Fig. 9a, c).

The *GLR2::BELL1* complementation line was generated by homologous recombination using the *glr1/2* knockout background. A construct containing the *BELL1* coding sequence followed by the Tnos terminator sequence and the zeocin-resistant cassette was inserted *in situ* immediately downstream of the *GLR2* promoter, which resulted in the replacement of the genomic region containing the hygromicin-resistant cassette. The vector used for transformation, pZB1, was generated as follows: The coding region of *BELL1* was amplified by PCR from mature sporophyte cDNA with the primers oCR025/oCR026 and cloned into pBNRF plasmid using XhoI and SalI restriction enzymes. Subsequently, the upstream flanking genomic region of the *GLR2* gene was amplified using the primers oCR029/oCR030 and cloned into the same plasmid using AvrI and SalI. A fragment containing the Tnos terminator followed by the zeocin-resistance cassette was amplified from the pTFH38.9C plasmid with the primers oCR032/oCR033 and cloned into pBNRF using XhoI and ApaI, replacing the G418-resistance cassette. The resulting plasmid was renamed pZB1. Finally, the downstream flanking genomic region of *GLR2* was amplified with the primers oCR010/oCR011 and cloned into pZB1 using ApaI and AscI (Extended Data Fig. 9b). The plasmid was linearized for the transformation of *glr1/2-11* double-knockout protoplasts. The selection of zeocin-resistant colonies was done as before and stable colonies were genotyped to confirm correct insertion (Extended Data Fig. 9d). Three independent lines were obtained (*GLR2::BELL1-18*, *GLR2::BELL1-57* and *GLR2::BELL1-10*). All lines were analysed showing similar phenotypes (Extended Data Fig. 8c, d). Results presented in the main text were obtained using *GLR2::BELL1-18*.

Assessment of protonema growth under different [Ca^{2+}]. For determining protonema growth, small pieces (around 1 mm in diameter) of recently grinded tissue (5 days after the last grinding propagation) were plated in modified KNOPS medium supplemented with different calcium concentrations. For the preparation of such medium, the concentration of $Ca(NO_3)_2$ was reduced and substituted for KNO_3 as a source of nitrogen. Standard used agar (Formedium agar) was also substituted by purified agar with low content of residual Ca^{2+} (Sigma A7921). Pictures of protonema colonies were taken at days 0 and 5. Protonema growth was estimated as the change in colony diameter from day 0 to 5. Results are presented as average change in colony diameters.

Measurements of caulonema length. For induction of caulonema filaments fresh protonema was grown for 7 days under long-day conditions. After this period, protonema was collected using forceps and then distributed forming horizontal lanes in a Petri dish with KNOPS medium and a cellophane layer. The plate was covered with aluminium foil to create dark conditions and placed on a vertical position (caulonema is known to grow negatively to the gravity vector) at 25 °C for 5 days. Finally, caulonema were measured longitudinally from the tip of the filament until the first branch at the base. ImageJ was used to calculate distance.

Quantification of sporophyte production rates. Induction of gametangia was conducted after 28 days of growth on sterile peat pellets (Jiffy-7; Jiffy Products). The phenotyping of the lines was done once the sporophytes reached the mature stage (6 weeks after gametangia induction). Fertility rates (percentage of gametophores with sporophytes) were assessed by counting successfully developed sporophytes in at least 100 randomly collected gametophores per sample. Previous characterization of fertility rates in the wild type showed that under our conditions, sporophyte production rates were between 45 and 60%. Furthermore, we observed that samples with lower production rates always showed defects such as fungus or bacteria contamination, or low humidity. Therefore samples from both genotypes with fertility rates below 45% were discarded for statistical analysis, considered as stress affected. Statistical differences between samples were estimated using a Student's *t*-test or Wilcoxon–Mann–Whitney test as needed.

Cross-fertilization experiments. Protonema tissue from the two strains being crossed was collected in approximately equal amounts and placed on a glass container with water. Tissue was grinded with a tissue disrupter (TissueRuptor; Qiagen) and transfered to sterile peat pellets (Jiffy-7; Jiffy Products) in plastic containers. Gametophores were grown and exposed to gametangia inducing conditions as described before. 15 days after transfer, approximately 30 ml of tap water was added to the top of the gametophore mesh. This step was repeated three times to ensure water reached most of the gametophores. On the next day, the procedure was repeated and excess water was decanted. Samples continued under gametangia inducing conditions for 3–4 weeks. After this period, sporophytes were visualized under a fluorescent stereomicroscope (Zeiss Stereo Lumar).

Visualization and collection of *Physcomitrella* reproductive organs. Reproductive organs (antheridia and archegonia) were manually isolated from gametophore apexes under a stereomicroscope using very fine forceps (Dumoxel-biology 5; Electron Microscopy Sciences). For visualization samples were placed on a microscope slide with water and images were acquired on an upright microscope (Leica DM LB2; Leica Microsystems), equipped with a colour camera (UI-3370CP Rev.2, IDS) using a 20× objective with bright-field illumination. For RNA extraction, isolated reproductive organs were collected directly into trizol

reagent. RNA purification for cDNA synthesis was done as described before and used for microarray hybridization.

Quantification of spore size and numbers. Spores were obtained by bursting mature sporophytes into sterile water. In the case of wild type, *glr1* and *glr2*, the content of three mature sporophytes was released in 250 µl of sterile water. Since *glr1/2* had fewer spores, the contents of three sporophytes were released in 100 µl of water to keep adequate spore densities. To calculate the spore two-dimensional area, pictures were taken with an inverted microscope (Leica DMRA2, Leica Microsystems) using a 20× objective with bright-field illumination and measured using ImageJ 'measuring' function (http://imagej.nih.gov/ij/). Determination of the number of spores per sporophyte was done by taking 10 µl of the samples containing spores (prepared as mentioned before) and placing them on a haemocytometer chamber (NeuBauer Blaubrand, Sigma-Aldrich). Both upper and lower grids were used for counting. Each sample was measured three times to minimize variation.

Microarray hybridization and data analysis. Approximately 750 ng of cDNA was used for labelling and hybridization on custom Nimblegen 12×135K arrays (Roche NimbleGen) following manufacturer's instructions in the IRB Barcelona Functional Genomics Core Facility (FGC). Arrays were scanned and raw data were obtained using the DEVA software, applying robust multichip average (RMA) normalization to all arrays (Roche NimbleGen). Differential expression analysis was conducted using dChip software[28] (http://www.hsph.harvard.edu/cli/complab/dchip/). Data were imported as 'external data' in tab-delimited text format, including expression data and standard error. To determine differentially expressed genes, pair-wise comparisons between *glr1/2* and wild-type samples were conducted. To obtain the list of downregulated genes in *glr1/2* reproductive organs with respect to wild type, we used a lower-confidence bound fold-change (LCB FC) cut-off of 3. A total of 11 genes were obtained using this stringent cut-off. Information about gene function was obtained from the *P. patens* annotation v1.6 release 2012.3 (http://www.cosmoss.org), combined with information from several alignments against non-plant organisms and STRING information.

Determination of sperm cell swimming behaviour. To quantify the number of sperm cells that successfully target the archegonia entrance, reproductive units were isolated from gametophores exposed to gametangia inducing conditions for 15 days. One intact reproductive unit was isolated (the entire set of archegonia and antheridia produced at the tip of one gametophore) and placed in a 35 mm glass bottom dish (Nunc, Thermo Fisher) containing 60 µl of sperm medium composed of 0.45 mM $CaCl_2$, 0.3 mM $MgSO_4$, 0.02 mM KNO_3 and 0.081 $NaHCO_3$. After sperm cells were released from the antheridia (typically one cluster of sperm cells per sample was released), the archegonia entrance was monitored for 45 min and time-lapse image acquisition was done every time a sperm cell was spotted swimming close to the archegonium. Monitoring of the sample and time-lapse images were acquired on a High Content Screening (HCS) inverted microscope (Leica HCS; Leica Microsystems) equipped with a sCMOS camera (Flash Orca LT 4.0; Hamamatsu, Japan) at 80 frames per second, and using a 20× objective with bright-field and differential interference contrast (DIC) illumination.

To determine differences in the swimming behaviour of sperm cells, reproductive units were isolated and placed under the same conditions as before. Time-lapse imaging was done after the sperm cells managed to free themselves from the protein matrix and started swimming freely in the medium. Tracking of their two-dimensional paths and calculation of different swimming parameters were done using the ImageJ 'manual tracking' plugin.

Measurements of cytoplasmic [Ca^{2+}] in sperm cells. Sperm cells were incubated in 60 µl of sperm medium (0.45 mM $CaCl_2$, 0.3 mM $MgSO_4$, 0.02 mM KNO_3 and 0.081 $NaHCO_3$) containing 10 µM Fluo-4-AM for 1 h. Medium also contained a high number of archegonia. Images were acquired on a high content screening (HCS) inverted microscope (Leica HCS; Leica Microsystems) equipped with a sCMOS camera (Flash Orca LT 4.0; Hamamatsu), under a 20×/NA1.2 water immersion objective. Fluorescent images were acquired with a 488 nm excitation wavelength and 525/36 nm emission filter. Image analysis and quantification followed protocols and principles established elsewhere[29]. In short, fluorescence profiles were manually extracted using line segments to average across 7 pixels width using ImageJ, including the neighbouring background. Cells outside of regions prone to artefacts and distortions were selected based on a minimum visible fluorescence from two independent inductions per genotype. Local polynomial fits with different coarseness were performed in the raw fluorescence profiles to estimate the background and subtract it from the signal. Fluorescence peaks of individual cells were extracted from the fine-grained smoothing having the background, estimated from the coarse-grained smoothing, subtracted to yield the normalized Ca^{2+} signal.

Gene network analysis. Gene network analysis of *GLR1* and *GLR2* was done using the PlaNET tool (http://aranet.mpimp-golm.mpg.de/index.html). Networks were constructed using the HCCA algorithm with expression data for *P. patens* available in the PlaNET database (default parameters). Each network consists of genes located two steps away from the query gene. Functional enrichment analysis was done using the DAVID Bioinformatics Resources 6.7 (https://david.ncifcrf.gov)[30] based on *Arabidopsis thaliana* homologue genes. Genes were clustered according to their Gene Ontology terms, including biological process, molecular function, and cellular component. Enrichment scores were calculated on the basis of the EASE scores (modified Fisher exact *P* value) of each cluster term member. Default parameters were used for the analysis.

Statistics. Minimal sample size estimation was calculated using the Soper D. Statistics Calculators version 4.0 (http://www.danielsoper.com/statcalc/default.aspx) to ensure a statistical power level of at least 0.7, a Cohen's *d* of 0.5, and a probability of 0.05 for a two-tailed *t*-test. Technical challenges of tracking sperm cell mobility and determining electrophysiological properties of GLRs imposed sample size restrictions; therefore, sample size estimation was not calculated for experiments shown in Figs 2 and 4. However, we estimated the effect size taking into account the mean and standard deviation of samples used for these experiments using the Ellis PD effect size calculators (http://www.polyu.edu.hk/mm/effectsizefaqs/calculator/calculator.html). For all comparisons shown in Fig. 2, the effect size was at least 0.8 (Cohen's *d*), which is considered a large effect.

Unpaired sample *t*-tests were used to compare wild-type versus single- or double-knockout mutant samples. In all cases, only two groups were compared at a single time. Variance, normality and *P* values were calculated using the Sigma Plot 11 software package (https://systatsoftware.com/products/sigmaplot/). Unequal variances approach was applied as necessary by the software. In cases in which data were not normally distributed, the non-parametric Mann–Whitney *U* test was used. Alternatively the statistical programming language R was used to perform Welch's unequal variances *t*-test, local polynomial fits and violin plots.

Data availability. Microarray raw and normalized data can be accessed in the array express database (https://www.ebi.ac.uk/arrayexpress/), accession number E-MTAB-5268. Source data are provided for Fig. 1d, c, 2b–f, i, 3b, c, 4d, f, h and Extended Data Figs 1e, 4b, d, 5b, d, f, 6b, d, f, h. Uncropped gels for gel images presented in Extended Data Figs 7 and 9 are provided in the Supplementary Information. All other data are available from the corresponding author upon reasonable request.

23. Ashton, N. & Cove, D. The isolation and preliminary characterisation of auxotrophic and analogue resistant mutants of the moss, *Physcomitreila patens*. *Mol. Genet. Genomics* **154,** 87–95 (1977).
24. Reski, R. & Abel, W. O. Induction of budding on chloronemata and caulonemata of the moss, *Physcomitrella patens*, using isopentenyladenine. *Planta* **165,** 354–358 (1985).
25. Hohe, A., Rensing, S. A., Mildner, M., Lang, D. & Reski, R. Day length and temperature strongly influence sexual reproduction and expression of a novel MADS-box gene in the moss *Physcomitrella patens*. *Plant Biol.* **4,** 595–602 (2002).
26. Reyes, R. *et al.* Cloning and expression of a novel pH-sensitive two pore domain K^+ channel from human kidney. *J. Biol. Chem.* **273,** 30863–30869 (1998).
27. Jurman, M. E., Boland, L. M., Liu, Y. & Yellen, G. Visual identification of individual transfected cells for electrophysiology using antibody-coated beads. *Biotechniques* **17,** 876–881 (1994).
28. Li, C. & Wong, W. H. Model-based analysis of oligonucleotide arrays: expression index computation and outlier detection. *Proc. Natl Acad. Sci. USA* **98,** 31–36 (2001).
29. Damineli, D. S. C., Portes, M. T. & Feijó, J. A. Oscillatory signatures underlie growth regimes in *Arabidopsis* pollen tubes: computational methods to estimate tip location, periodicity, and synchronization in growing cells. *J. Exp. Bot.* **12,** 3267–3281 (2017).
30. Huang, W., Sherman, B. T. & Lempicki, R. A. Systematic and integrative analysis of large gene lists using DAVID bioinformatics resources. *Nat. Protocols* **4,** 44–57 (2009).

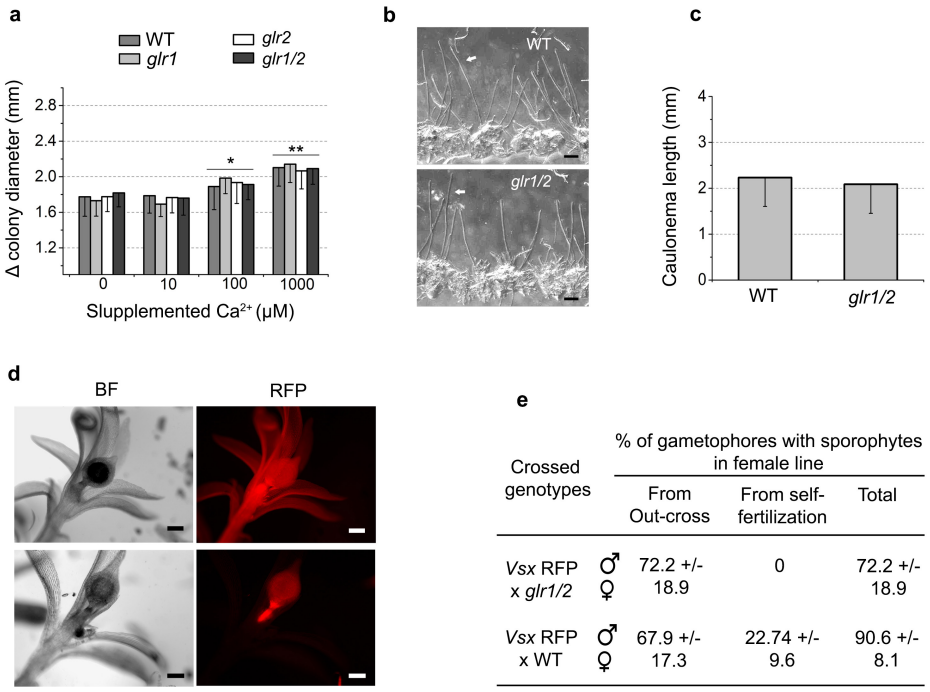

e

Crossed genotypes		% of gametophores with sporophytes in female line		
		From Out-cross	From self-fertilization	Total
Vsx RFP ♂ x *glr1/2* ♀		72.2 +/- 18.9	0	72.2 +/- 18.9
Vsx RFP ♂ x WT ♀		67.9 +/- 17.3	22.74 +/- 9.6	90.6 +/- 8.1

Extended Data Figure 1 | Measurement of caulonema filaments and cross-fertilization. a, Growth of protonema colonies under different Ca^{2+} concentrations. The initial colony diameter was subtracted from the diameter at day 5. Data are from 3 biological replicates and several independent colony measurements. $n = 59$ (WT), $n = 58$ (*glr1*), $n = 58$ (*glr2*) $n = 55$ (*glr1/2*). Error bars denote s.d. There was a statistically significant difference between Ca^{2+} treatments ($P < 0.001$, $F_{156.3}$, two-way ANOVA) but not between genotypes ($P = 0.952$, two-way ANOVA). Colony diameter in samples treated with 100 and 1,000 μM Ca^{2+} was significantly different from untreated samples. $^{*}P = 0.01$, $^{**}P < 0.001$, Holm–Sidak multiple comparison test. **b**, Caulonema cells (white arrows) from wild-type lines and the *glr1/2* mutant have similar morphologies. Scale bars, 500 μM. Images are representative of 13 images. **c**, Caulonema length from filaments induced in darkness. There was no significant difference between the wild type ($n = 148$) and *glr1/2* mutant ($n = 180$). Error bars represent s.d. Results were obtained from 3 biological replicates. **d**, Self-fertilization events (top) and outcrossing events (bottom) were identified in cross-fertilization experiments between *Vsx* RFP (paternal line) and *glr1/2* (maternal line). Scale bars, 200 μm. Images are representative of 4 images. **e**, Sporophyte production rates in cross-fertilization experiments using different genotypes are shown. Sporophyte production in *glr1/2* was as high as in the wild type (outcrossing rates), suggesting full phenotypic complementation when *Vsx* sperm cells are provided. 50 gametophores per replicate were analysed. Data are mean ± s.d. from 4 biological replicates.

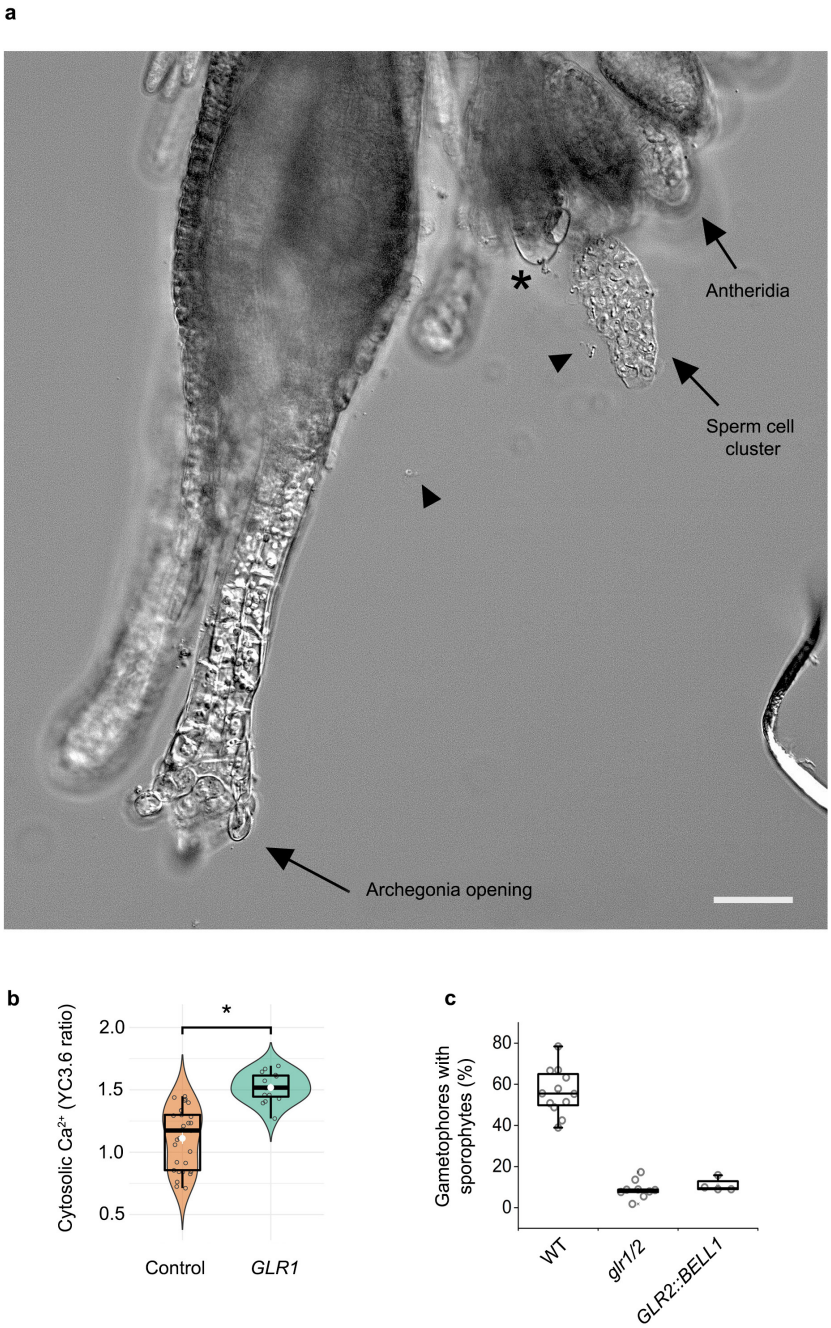

Extended Data Figure 2 | Display of an isolated reproductive unit, and quantification of cytosolic calcium and sporophyte production. a, An intact open archegonium, several antheridia, and a sperm cell cluster are shown (arrows). In most samples, only one antheridium was ready to release the sperm cells at the time of the experiment. The antheridium from which the sperm cell cluster was released is indicated by an asterisk. After 1 min, the released sperm cells became fully motile and individual cells began to separate from the protein matrix (arrowheads). Scale bar, 30 μm. Image is representative of 6 images. **b**, Basal cytosolic calcium in control cells (transfected with pCI and pEF1-YC3.6) and cells co-expressing GLR1 and YC3.6 exposed to medium with no calcium. $n = 29$ (control), $n = 15$ (GLR1); biological replicates. There was a statistically significant difference between the two samples. $^*P = 3 \times 10^{-8}$, Welch's *t*-test for unequal variances. Violin plots show curves of density estimates, boxplots and white points with lines are mean and s.e.m. **c**, The *GLR2::BELL1* complementation line shows a similar sporophyte production rate to the *glr1/2* mutant line. The percentage of gametophores with sporophytes from the total number of gametophores is shown. Data are mean ± s.d. from several independent biological replicates. $n = 12$ (WT), $n = 7$ (*glr1/2*), $n = 4$ (*GLR2::BELL1*). 100 gametophores were counted per sample. Box plot lines show outliers.

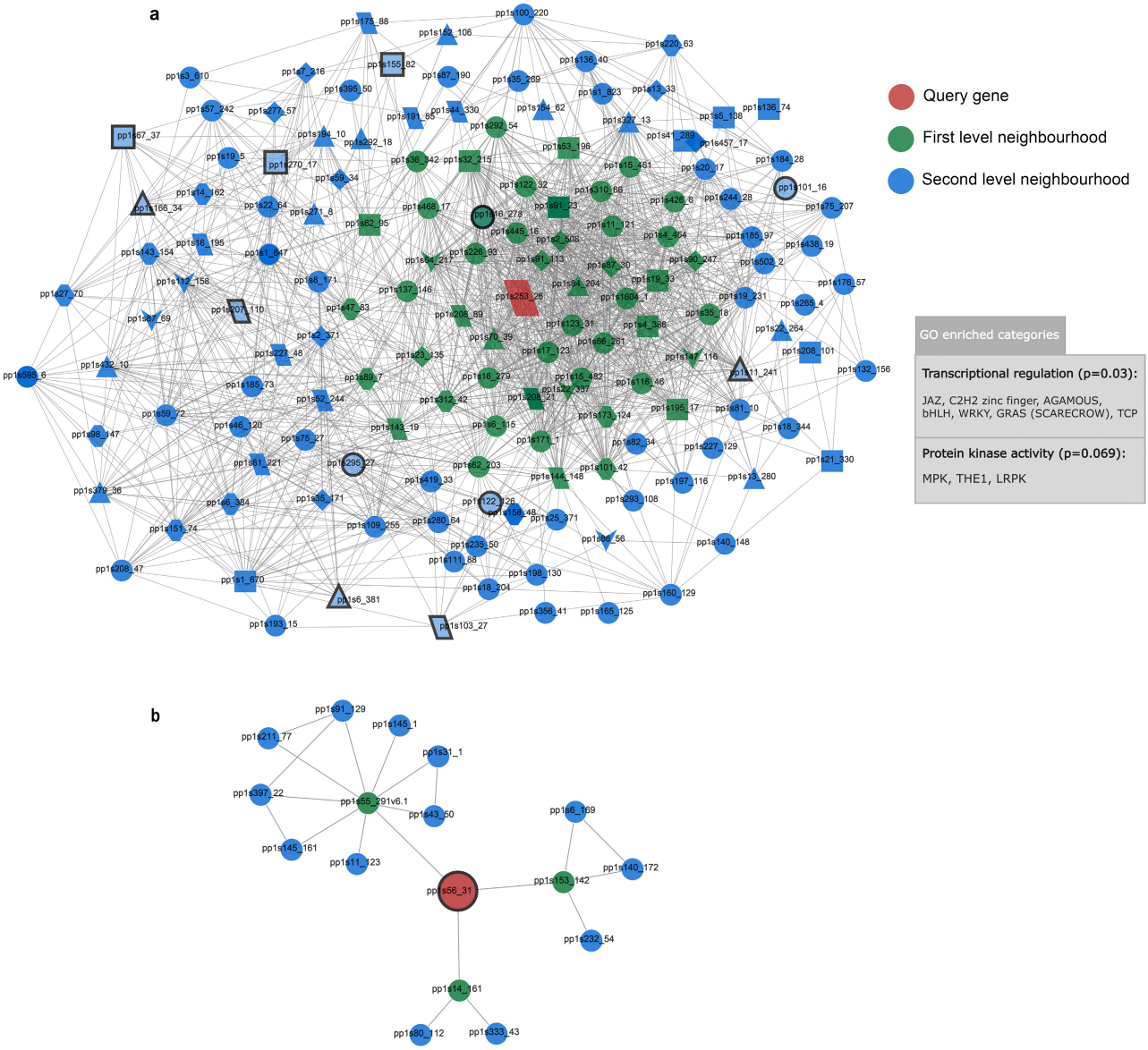

Extended Data Figure 3 | Gene network analysis for *GLR1* and *GLR2*. **a**, *GLR2* co-expression gene network showing genes one and two steps away from the query gene. Gene Ontology (GO) analysis of the 151 genes that integrate the network shows only two enriched categories: transcriptional regulation and protein kinase activity (modified Fisher exact *P* value). The gene families represented in the two clusters are shown in italics. Highlighted nodes represent transcription factors genes interacting with *GLR2* in the network. **b**, *GLR1* co-expression gene network showing genes two steps away from the query gene. No enriched Gene Ontology categories were found. *GLR1* is highlighted at the centre of the network. Shapes represent label co-occurrences used to group genes according to Pfam domains and PLAZA families. See Supplementary Table 3 for the complete gene lists and annotations.

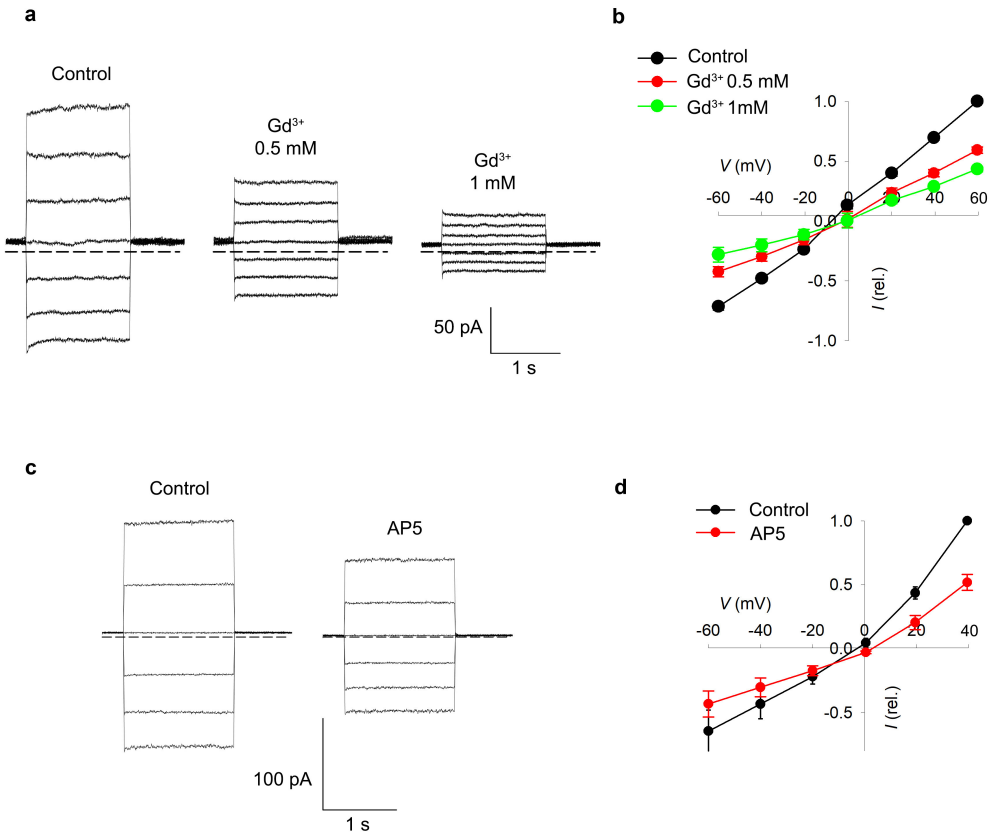

Extended Data Figure 4 | Effect of Gd^{3+} and AP5 on 35S::PpGLR1 protoplasts currents. a, Typical currents recorded in protoplasts from 35S::PpGLR1 protonema under the whole-cell configuration before and after the application of 0.5 and 1 mM Gd^{3+}. **b**, Standardized current–voltage curves of stationary currents recorded in experiments as shown in **a**. $n = 3$ for all conditions. **c**, Effect of AP5 (200 μM) on typical currents recorded in protoplasts from 35S::PpGLR1 ($n = 5$). **d**, Standardized currents corresponding to **c**, recorded before (black circles) and after (red circles) the addition of 200 μM AP_5 ($n = 4$). In all cases n represents biological replicates. Error bars denote s.e.m.

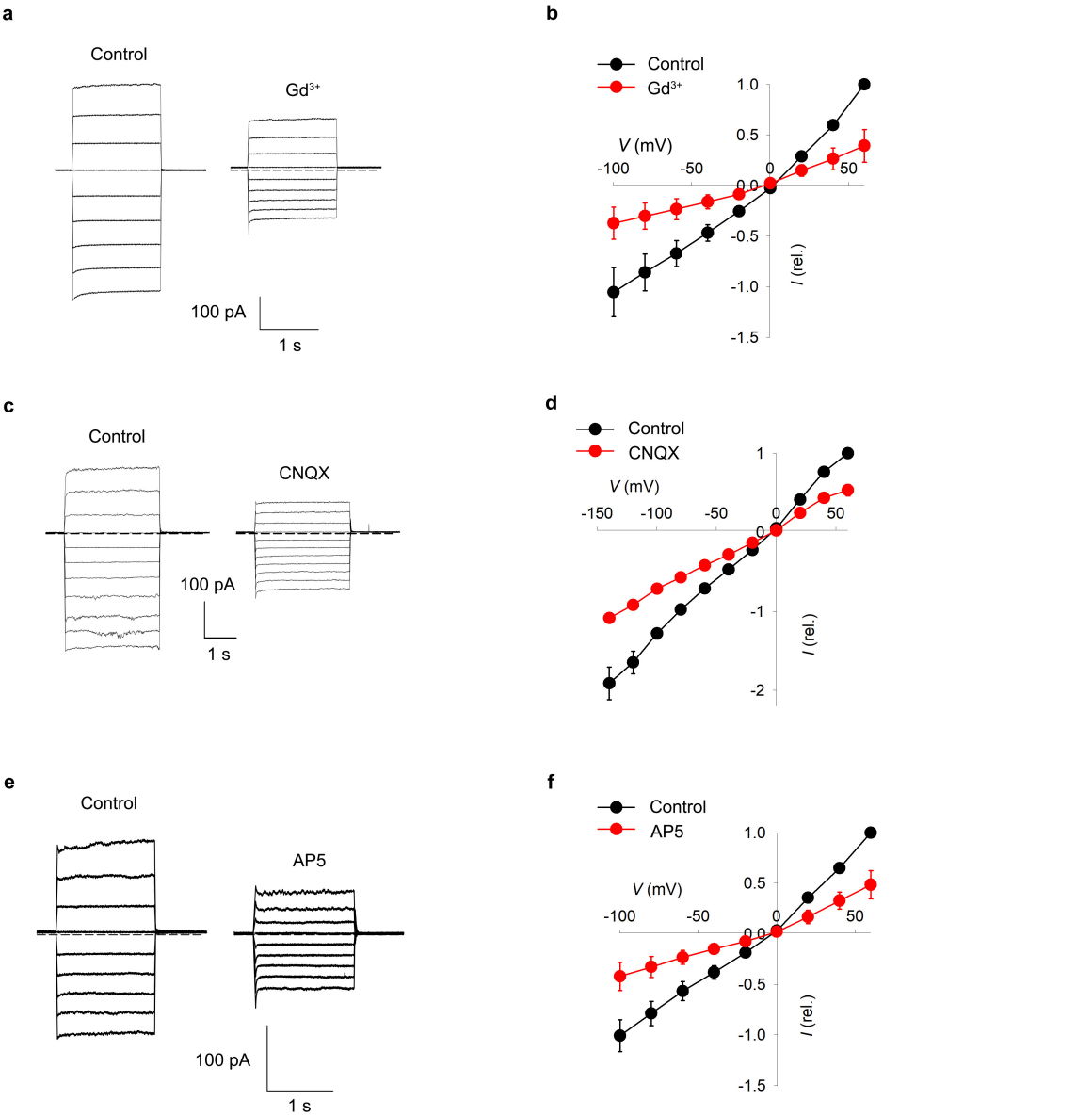

Extended Data Figure 5 | Effect of Gd^{3+}, CNQX and AP5 on COS-7 cells expressing GLR1. a, Typical currents recorded in COS-7 cells transfected with pCI-PpGLR1 before and after the addition of 1 mM Gd^{3+}. **b**, Standardized current–voltage curves of experiments in **a**. Currents were recorded in control conditions before Gd^{3+} application (black circles), and after the addition of 1 mM Gd^{3+} (red circles) ($n = 3$ for control and treatment). **c**, Typical currents recorded in transfected COS-7 cells expressing GLR1 in control solution (left) and after the addition of 50 μM CNQX (right). **d**, Standardized current–voltage curves of experiments in **c**. Currents were recorded in control conditions (black circles), and after the addition of 50 μM CNQX (red circles) ($n = 3$). **e**, Typical currents recorded in COS-7 cells transfected with pCI-PpGLR1 before and after the addition of AP_5 (200 μM). **f**, Standardized current–voltage curves of experiments presented in **e**. Currents were recorded in control conditions (black circles) and after the addition of 200 μM AP_5 (red circles) ($n = 4$). Standard solutions are identical to Fig. 4e, f. Pipette contained 146 mM Cl^- and 140 mM Na^+, bath solution contained 150 mM Cl^-, 5 mM Ca^{2+} and 10 mM Na^+ as charge carriers. Error bars denote s.e.m. In all cases *n* represents biological replicates.

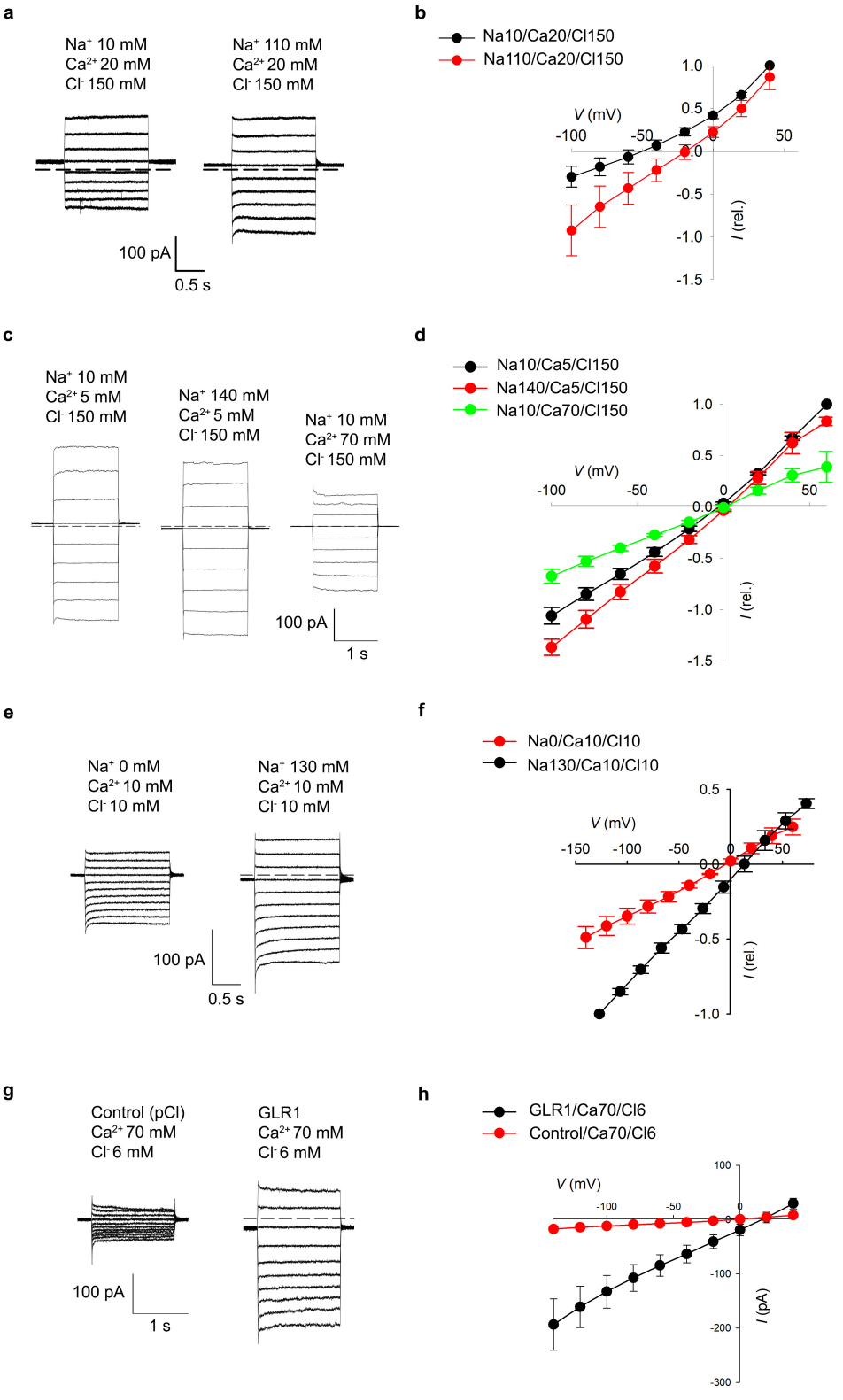

Extended Data Figure 6 | See next page for caption.

Extended Data Figure 6 | GLR1 is a non-selective channel. a, Typical currents recorded in wild-type protoplasts from protonema with 10 or 110 mM Na^+. **b**, Standardized current–voltage curves of experiments in **a**. 10 mM Na^+ (black circles), 110 mM Na^+ (red circles) ($n = 4$). **c**, Typical currents recorded in COS-7 cells transfected with pCI-PpGLR1 with external solutions containing: (i) 10 mM Na^+, 5 mM Ca^{2+}, 150 mM Cl^-; (ii) 140 mM Na^+, 5 mM Ca^{2+}, 150 mM Cl^-; or (iii) 10 mM Na^+, 70 mM Ca^{2+}, 150 mM Cl^-. **d**, Standardized current–voltage curves of experiments presented in **c** ($n = 3$). **e**, Representative current traces from COS-7 cells transfected with pCI-PpGLR1 in an external solution containing 10 mM Ca^{2+} and 10 mM Cl^- without Na^+ (left) and with 130 mM Na-gluconate (right) applied by perfusion. Pipette solutions were as in Fig. 4g, h. **f**, Standardized current–voltage curves of experiments shown in **e**. Na^+-free solutions (red circles), 130 mM Na^+ (black circles) ($n = 3$). When the external Na^+ concentration increased from 10 to 140 mM, a current increase was observed, demonstrating the permeability of GLR1 for Na^+ shown in **c** and **d**. Furthermore, Na^+ permeability was confirmed as the current intensity increased and the reversal potential also significantly shifted to the right when adding Na^+ to the external solution, as shown in **e** and **f**. **g**, Representative current traces from control cells (left) and COS-7 cells transfected with pCI-PpGLR1 (right) in 70 mM Ca^{2+} bathing solution (experimental conditions as in Fig. 4g, h). **h**, Current–voltage curve depicting average stationary current intensity as shown in **g**. Control (red circles) and pCI-PpGLR1(black circles) ($n = 3$). The increase in current by external Ca^{2+} demonstrates a permeability of GLR1 to Ca^{2+}. Together with data presented in **c** and **d**, these results suggest a complex effect of external Ca^{2+}. Indeed, while **g** and **h** demonstrate a Ca^{2+} permeation in conditions in which no Na^+ and low (6 mM) Cl^- are present, **c** and **d** show a decrease of ionic currents by high extracellular Ca^{2+} when the bath contains 10 mM Na^+ and 150 mM Cl^-. Panels **e**–**h** also suggest that Cl^- may pass through the channel accounting for the portion of outward current. Error bars denote s.e.m. In all cases *n* represents biological replicates.

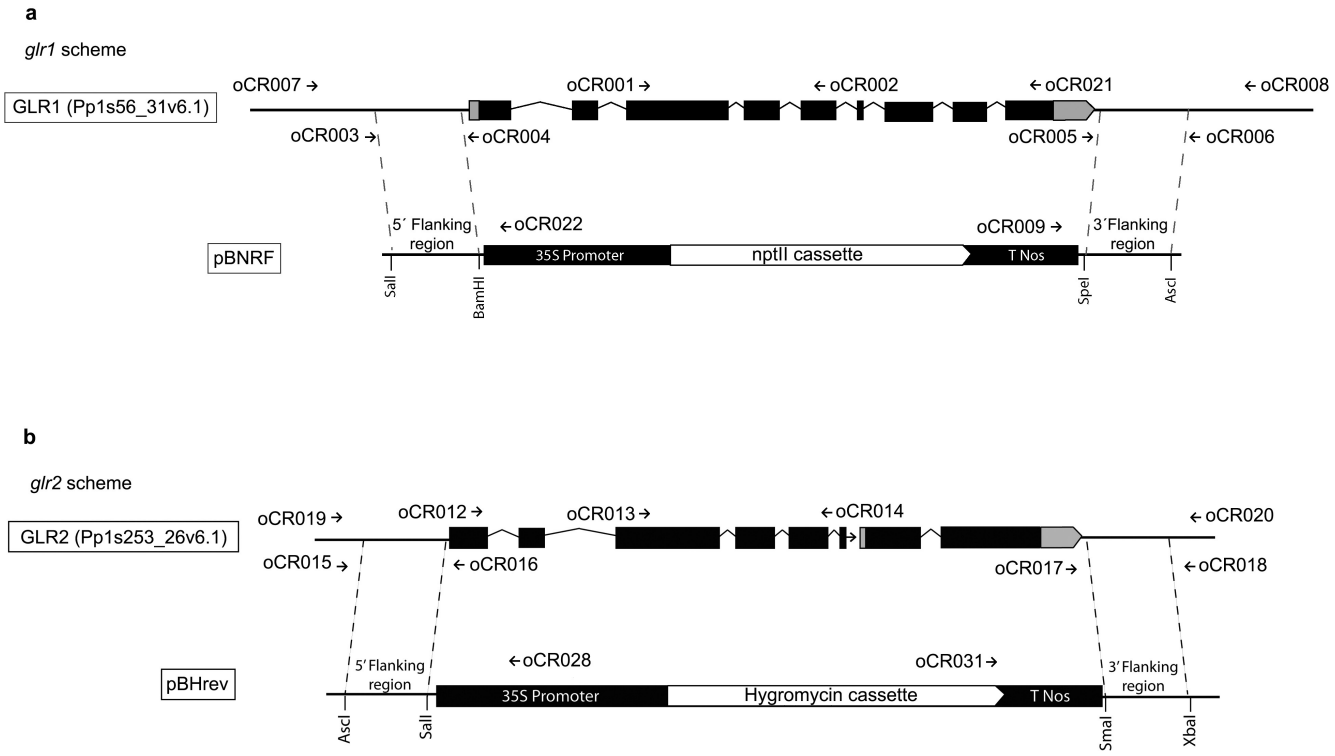

Extended Data Figure 7 | Schematic representation of the constructs used for the generation of *glr1* and *glr1/2* mutants by homologous recombination. a, *GLR1* endogenous genomic locus (top) and pBNRF plasmid used for transformation (lines) are shown. The boxes and lines between the boxes represent exons and introns, respectively. Grey boxes represent untranslated regions (UTRs) of the gene, and small arrows indicate the approximate position where primers bind to the DNA sequence. Broken lines denote the flanking genomic regions of the genes used for homologous recombination. **b**, The endogenous genomic locus of *GLR2* (top) and the pBHrev construct used for transformation (bottom). **c**, PCR showing deletion of the *GLR1* gene from *glr1* knockout mutants and the correct insertion of the construct used for transformation. **d**, Same as **c** but for the *glr1/2* double-knockout mutants. See Supplementary Information for uncropped gel images.

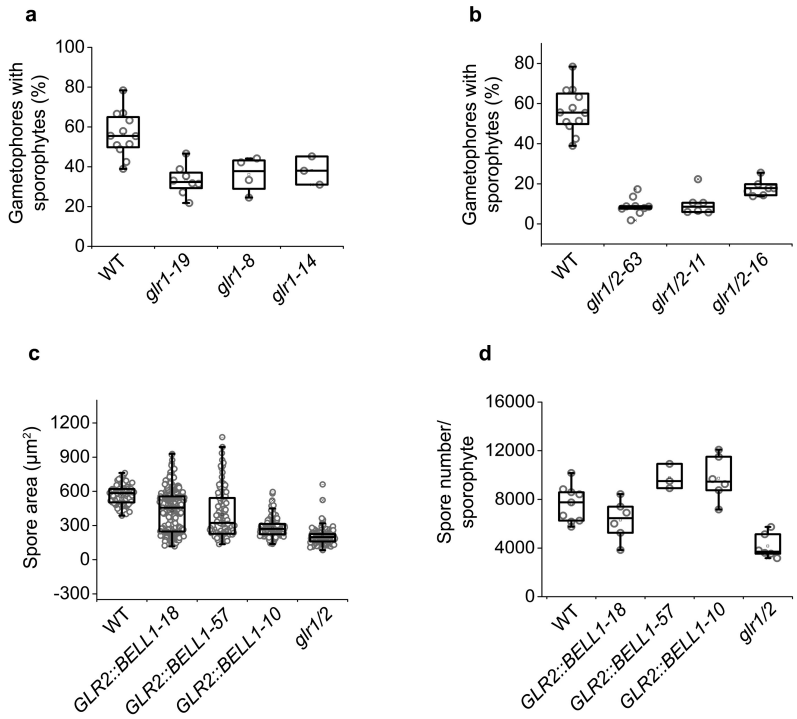

Extended Data Figure 8 | Independent mutant lines have similar phenotypes. a, All *glr1* mutant lines show a significant difference in sporophyte production when compared to wild-type lines. $P \leq 0.012$, two-tailed *t*-test. 100 gametophores were counted per sample (biological replicates); $n = 12$ (WT), $n = 8$ (*glr1-19*), $n = 4$ (*glr1-8*), $n = 3$ (*glr1-14*). **b**, Similarly, all *glr2* mutant lines produced very few sporophytes compared to wild-type lines. $P \leq 0.004$, Mann–Whitney *U*-test. Data from several biological replicates; $n = 12$ (WT), $n = 9$ (*glr1/2-63*), $n = 7$ (*glr1/2-11*), $n = 4$ (*glr1/2-16*). 100 gametophores were counted per sample. **c**, All complementation lines had significantly bigger spores than spores of *glr1/2* double-knockout lines. $P \leq 0.001$, Mann–Whitney *U*-test. Spores from 3 biological replicates were pooled and measured. Data points represent individually measured spores. $n = 82$ (WT), $n = 174$ (*glr1/2*) $n = 117$ (*GLR2::BELL1-57*), $n = 284$ (*GLR2::BELL1-18*), $n = 202$ (*GLR2::BELL1-10*). **d**, Similarly, *GLR2::BELL1* sporophytes clearly produced more spores than *glr1/2* mutants ($P \leq 0.022$, two-tailed *t*-test). Data from several biological replicates. $n = 9$ (WT), $n = 6$ (*GLR2::BELL1-18*, *GLR2::BELL1-10*, *glr1/2*), $n = 3$ (*GLR2::BELL1-57*). Box plots show 25th and 75th percentiles, and lines indicate outliers.

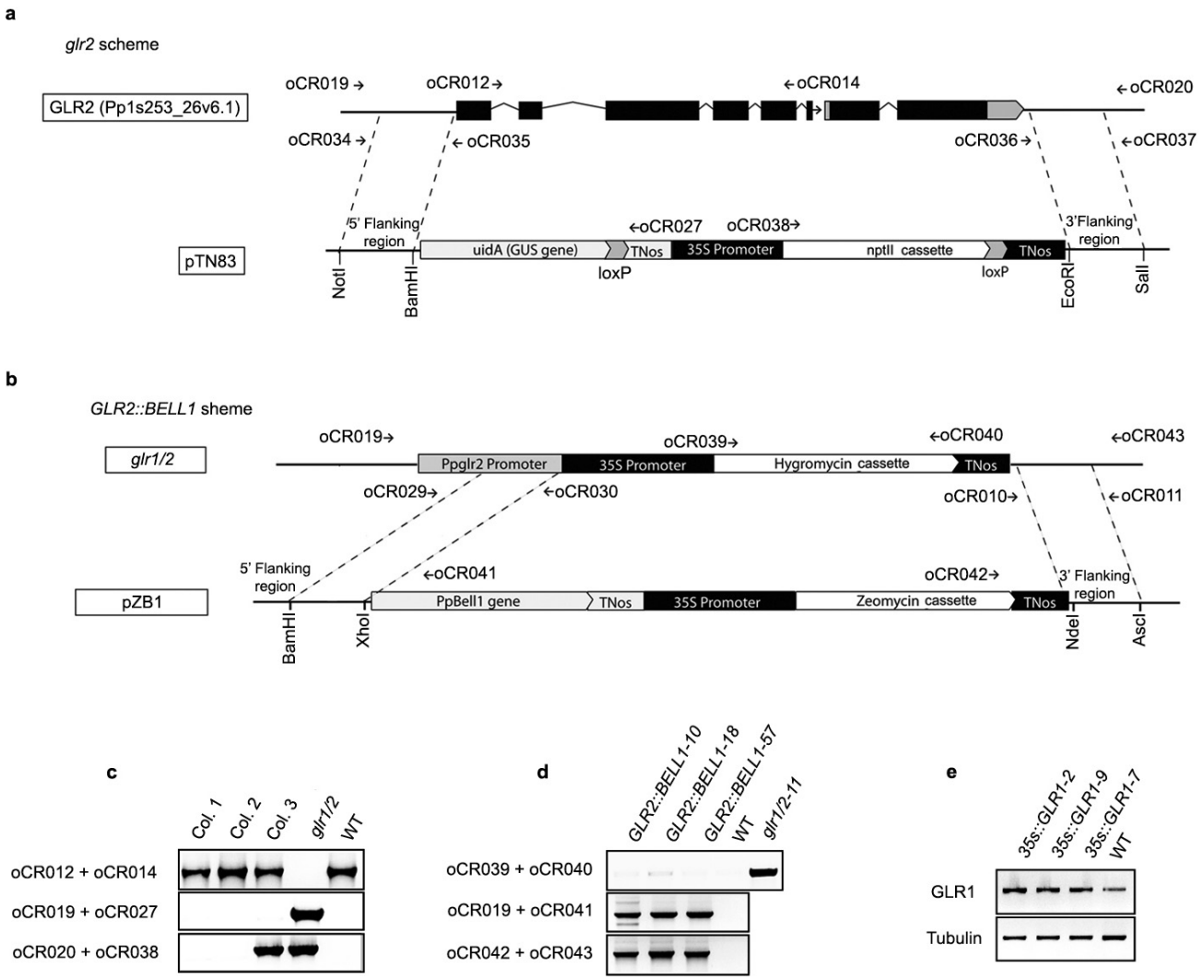

Extended Data Figure 9 | Schematic representation of the constructs used for the generation of *glr2* and *GLR2::BELL1* mutants by homologous recombination. a, *GLR2* endogenous genomic locus (top) and pTN83 plasmid used for transformation (bottom). The boxes and lines between the boxes represent exons and introns, respectively. Small arrows indicate the approximate position where primers bind to the DNA sequence. Broken lines denote the genomic regions used for homologous recombination. **b**, The endogenous genomic locus in the *glr1/2* mutant (top), and pZB1 construct used for transformation (bottom). **c**, PCR showing the deletion of the *GLR2* gene from *glr2* single-knockout mutants and the correct insertion of the construct used for transformation. **d**, Hygromycin could not be detected in *GLR2::BELL1* complementation mutants and PCR analyses show correct insertion of the construct. **e**, RT–PCR experiments show that *GLR1* transcripts are more abundant in 35S::PpGLR1 lines. 25 cycles of PCR amplification using cDNA obtained from protonema were used to amplify *GLR1* in wild-type and overexpression lines. α-tubulin (*TUB*) was used as a control. See Supplementary Information for uncropped gel images.

Extended Data Table 1 | Differentially expressed genes in *glr1/2*

Gene ID	Fold change	At homolog	Description
Pp1s56_31V6	-67.37	GLR3.3	Glutamate receptor
Pp1s253_26V6	-38.14	GLR3.4	Glutamate receptor
Pp1s455_4V6	-8.35	n/a	polyphenol oxidase
Pp1s258_6V6	-7.69	BLH7	BELL1-like homeodomain
Pp1s79_259V6	-5.03	No homology	Oryza sativa GIL1, putative
Pp1s126_153	-6.06	No homology	
Pp1s18_45V6	-4.18	No homology	
Pp1s142_76V6	-3.96	No homology	
Pp1s385_31V6	-3.04	AAH	allantoate amidohydrolase
Pp1s252_5V6	-4.97	AT1G22900.1	Disease resistance-responsive

Microarray expression data from wild-type lines and the *glr1/2* mutant were used to generate a list of differentially expressed genes. The genes with the highest negative fold change (downregulated in *glr1/2* with respect to wild type) are presented.

nature research

Corresponding author(s): José A. Feijó

☐ Initial submission ☐ Revised version ☒ Final submission

Life Sciences Reporting Summary

Nature Research wishes to improve the reproducibility of the work that we publish. This form is intended for publication with all accepted life science papers and provides structure for consistency and transparency in reporting. Every life science submission will use this form; some list items might not apply to an individual manuscript, but all fields must be completed for clarity.

For further information on the points included in this form, see Reporting Life Sciences Research. For further information on Nature Research policies, including our data availability policy, see Authors & Referees and the Editorial Policy Checklist.

Experimental design

1. Sample size

Describe how sample size was determined.

Minimal sample size estimation was calculated using the Soper D. Statistics Calculators version 4.0 (http://www.danielsoper.com/statcalc/default.aspx) to ensure a statistical power level of at least 0.7, a Cohen´s d of 0.5, and a probability of 0.05 for a two-tailed t-test. For small samples, sample size effect was estimated taking into account the mean and standard deviation of samples used for these experiments using the Ellis PD. Effect size calculators (http://www.polyu.edu.hk/mm/effectsizefaqs/calculator/calculator.html).

2. Data exclusions

Describe any data exclusions.

There was no data exclusion from our statistical analyses. All samples were considered including those that deviated from the sample mean "outliers".

3. Replication

Describe whether the experimental findings were reliably reproduced.

For determining the sporophyte production rates (percentage of gametophore with sporophytes) one attempt out of 12, failed to replicate the expected production rate in wt and Ppglr1 genotypes. However, after close examination we determined that the mentioned batch of samples had fungi contamination and was not used for data collection. The rest of the experiments presented in the paper were successfully replicated.

4. Randomization

Describe how samples/organisms/participants were allocated into experimental groups.

No randomization method was used. Samples were not exposed to any treatments or stress conditions that deviate from what is considered the optimal growing conditions for Physcomitrella patens. Therefore randomized allocation of samples was not considered necessary. We rather focused on sample comparability, being careful to expose all the samples (genotypes) and experimental groups (single batch of samples or genotypes) to precisely the same growing and gametangia inducing conditions (i.e. temperature, light, humidity, nutrients, substract, growing material, examination conditions) for exactly the same amount of time. In addition, tissue dissection and data collection was performed after the same period of time for each of the replicates.

5. Blinding

Describe whether the investigators were blinded to group allocation during data collection and/or analysis.

Since we did not impose treatments or stress conditions in our sample groups, we didn't consider blinding to be necessary. Moreover, to ensure that samples from different genotypes were exposed to the same conditions we preferred to have them labeled with the genetic background information.

Note: all studies involving animals and/or human research participants must disclose whether blinding and randomization were used.

6. Statistical parameters

For all figures and tables that use statistical methods, confirm that the following items are present in relevant figure legends (or in the Methods section if additional space is needed).

n/a	Confirmed
☐	☒ The exact sample size (*n*) for each experimental group/condition, given as a discrete number and unit of measurement (animals, litters, cultures, etc.)
☐	☒ A description of how samples were collected, noting whether measurements were taken from distinct samples or whether the same sample was measured repeatedly
☐	☒ A statement indicating how many times each experiment was replicated
☐	☒ The statistical test(s) used and whether they are one- or two-sided (note: only common tests should be described solely by name; more complex techniques should be described in the Methods section)
☐	☒ A description of any assumptions or corrections, such as an adjustment for multiple comparisons
☐	☒ The test results (e.g. *P* values) given as exact values whenever possible and with confidence intervals noted
☐	☒ A clear description of statistics including central tendency (e.g. median, mean) and variation (e.g. standard deviation, interquartile range)
☐	☒ Clearly defined error bars

See the web collection on statistics for biologists for further resources and guidance.

Software

Policy information about availability of computer code

7. Software

Describe the software used to analyze the data in this study.	dChip v2010.01 software was used for microarray analysis and determination of differentially expressed genes. Origin 9.0 and Sigma Plot v12.2 were used for statistical analyses. Image J v2 was used for statistical analyses. No custom code was developed for this study.

For manuscripts utilizing custom algorithms or software that are central to the paper but not yet described in the published literature, software must be made available to editors and reviewers upon request. We strongly encourage code deposition in a community repository (e.g. GitHub). *Nature Methods* guidance for providing algorithms and software for publication provides further information on this topic.

Materials and reagents

Policy information about availability of materials

8. Materials availability

Indicate whether there are restrictions on availability of unique materials or if these materials are only available for distribution by a for-profit company.	There are no availability restrictions for material used in this study.

9. Antibodies

Describe the antibodies used and how they were validated for use in the system under study (i.e. assay and species).	NA

10. Eukaryotic cell lines

a. State the source of each eukaryotic cell line used.	NA
b. Describe the method of cell line authentication used.	NA
c. Report whether the cell lines were tested for mycoplasma contamination.	NA
d. If any of the cell lines used are listed in the database of commonly misidentified cell lines maintained by ICLAC, provide a scientific rationale for their use.	NA

Animals and human research participants

Policy information about studies involving animals; when reporting animal research, follow the ARRIVE guidelines

11. Description of research animals

Provide details on animals and/or animal-derived materials used in the study.	NA

Policy information about studies involving human research participants

12. Description of human research participants

Describe the covariate-relevant population characteristics of the human research participants.	NA